

Dynamics and transport properties of heavy fermions: Theory.

David E Logan and N S Vidhyadhiraja

University of Oxford, Physical and Theoretical Chemistry Laboratory,
South Parks Rd, Oxford OX1 3QZ, UK

Abstract. The paramagnetic phase of heavy fermion systems is investigated, using a non-perturbative local moment approach to the asymmetric periodic Anderson model within the framework of dynamical mean field theory. The natural focus is on the strong coupling Kondo-lattice regime wherein single-particle spectra, scattering rates, d.c. transport and optics are found to exhibit $(\omega/\omega_L, T/\omega_L)$ scaling in terms of a single underlying low-energy coherence scale ω_L . Dynamics/transport on all relevant (ω, T) -scales are encompassed, from the low-energy behaviour characteristic of the lattice coherent Fermi liquid, through incoherent effective single-impurity physics likewise found to arise in the universal scaling regime, to non-universal high-energy scales; and which description in turn enables viable quantitative comparison to experiment.

PACS numbers: 71.27.+a Strongly correlated electron systems; heavy fermions - 75.20.Hr Local moment in compounds and alloys; Kondo effect, valence fluctuations, heavy fermions

Submitted to: *J. Phys.: Condens. Matter*

1. Introduction.

Lanthanide based heavy fermion (HF) metals constitute a major, long studied class of correlated electron materials [1–8]. Their behaviour is quite distinct from conventional clean metals, the basic physics being driven by strong spin-flip scattering from essentially localised f -levels, generating the large effective mass and attendant low-energy scale indicative of strong interactions. The low-temperature (T) state is a lattice-coherent Fermi liquid with well defined quasiparticles and coherently screened f -spins, crossing over with increasing T to essentially incoherent screening via independent Kondo scattering, before attaining characteristic clean metallic behaviour. Physical properties of HF are in consequence typically ‘anomalous’: e.g. the resistivity $\rho(T)$ shows a strong non-monotonic T -dependence, while optics often exhibit rich structure from the microwave to the near infrared, and pronounced evolution on low temperature scales [1–8].

Theoretical treatments of HF centre on the periodic Anderson model (PAM), in which a non-interacting conduction band hybridizes locally with a correlated f -level in

each unit cell of the lattice; or on its strong coupling limit, the Kondo lattice model. The absence of exact results (save for some in one dimension, see e.g. [9]) has long spurred the search for suitable approximation schemes. One such framework, which has had a major impact in recent years, is provided by dynamical mean field theory (DMFT, for reviews see [10–13]). Formally exact in the large-dimensional limit, the self-energy within DMFT becomes momentum independent and hence spatially local, but still retains full temporal dynamics; such that all lattice models map onto an effective single-impurity model with a self-consistently determined host [10–13].

That raises an immediate question, easier asked than answered: to what extent are the properties of real HF materials captured within a DMFT approach to the PAM? To answer this clearly requires direct quantitative comparison of theory to experiment. And a prerequisite to that in turn is a method to solve the PAM — which DMFT does not *per se* provide. The latter has of course been studied extensively using a wide variety of techniques. Full scale numerical methods include the numerical renormalization group (NRG) [14, 15], quantum Monte Carlo [16–18] and exact diagonalization [19], while theoretical approaches encompass finite-order perturbation theory in the interaction U [20, 21], iterated perturbation theory [22, 23], the lattice non-crossing approximation [24, 25] and the average t -matrix approximation [26], large- N mean-field theory/slave bosons [27–29], the Gutzwiller variational approach [30, 31] and the recently developed local moment approach [32–34]. All of these methods naturally have their own virtues. But most possess significant, well known limitations [2], be it the general inability of perturbative approaches (and in practice quantum Monte Carlo) to handle strong interactions; failure to recover Fermi liquid behaviour at low-energies as arises in NCA-based approaches, restriction to the lowest-energy Fermi liquid behaviour as in large- N /slave boson mean-field theories, finite-size effects limiting exact diagonalization, and so on.

To enable viable comparison to experiment requires an approach that can adequately handle all experimentally relevant energy and/or temperature scales in the strongly correlated HF regime of primary interest; and indeed ideally also across the full spectrum of interaction strengths, such that intermediate valence and related behaviour can likewise be treated. One such is employed here, the local moment approach (LMA) [32–34]. Via study of the generic asymmetric PAM, our essential aims are (i) to provide a many-body description of dynamical and transport properties of paramagnetic HF, notably single-particle dynamics, d.c. transport and optical conductivities; as considered here. (ii) To make direct quantitative comparison with experiment. That is taken up in the following paper where comparison to transport/optical properties of CeB_6 , $CeAl_3$, $YbAl_3$ and $CeCoIn_5$ is made.

Some remarks on the LMA are apposite at this point since the paper will focus mainly on results obtained using the approach, with minimal technical details. Intrinsically non-perturbative and as such capable of handling strong interactions, the LMA [32–41] introduces the physically intuitive notion of local moments [42] from the outset. This leads directly to a ‘two-self-energy’ description in which, post mean-

field level, the key correlated spin-flip dynamics is readily captured; corresponding in physical terms to dynamical tunneling between initially degenerate local moment configurations, which lifts the erstwhile spin degeneracy and restores the local singlet symmetry characteristic of a Fermi liquid state. As with all techniques for lattice models within DMFT, the LMA originated in study of the single-impurity Anderson model (AIM) [35–41], where results for dynamics are known to give good agreement with NRG calculations [37, 38, 40], and for static magnetic properties with known exact results [41]. The approach has recently been developed to encompass the Anderson lattice (PAM); initially for the particle-hole symmetric limit [32, 33] appropriate to the Kondo insulating sub-class of heavy electron materials, where for all interaction strengths the system is an ‘insulating Fermi liquid’ that evolves continuously from its simple non-interacting limit of a hybridization-gap insulator [43]. From this a rich description of transport and optical properties of Kondo insulators arises [33], particularly in strong coupling where the system is characterized by an exponentially small indirect gap scale Δ_g , such that dynamics/transport exhibit scaling as functions of $(\omega/\Delta_g, T/\Delta_g)$. Exploiting that scaling enables direct comparison to experiment with minimal use of ‘bare’ material/model parameters; and in particular for three classic Kondo insulators $Ce_3Bi_4Pt_3$, SmB_6 and YbB_{12} , leads to what we regard as excellent agreement between theory and experiment on essentially all relevant energy and temperature scales [33].

The particle-hole symmetric PAM is of course special, confined as it is to the case of Kondo insulators. Most recently the LMA has been non-trivially extended to handle the generic asymmetric PAM [34] and hence HF metals (with the insulating symmetric limit recovered simply as a particular case). Single-particle dynamics at $T = 0$ were considered in [34], with a natural emphasis on the strongly correlated Kondo lattice regime of localised f -electrons but general conduction (‘ c ’) band filling n_c . The problem was found to be characterized by a *single* low-energy coherence scale ω_L — the precise counterpart of the insulating indirect gap scale Δ_g , and likewise exponentially small in strong coupling — in terms of which dynamics exhibit one-parameter universal scaling as a function of $\tilde{\omega} = \omega/\omega_L$, independently of either the interaction strength or local f/c hybridization. With increasing $\tilde{\omega}$ dynamics cross over from the low-energy quasiparticle behaviour required by and symptomatic of the coherent Fermi liquid state, to essentially incoherent single-impurity Kondo scaling physics at high- $\tilde{\omega}$ — but still in the $\tilde{\omega}$ -scaling regime and as such incompatible [34] with a two-scale ‘exhaustion’ scenario [44].

In this paper we extend the work of [34] to finite temperature, thereby enabling access to d.c. transport and optics. Our primary focus is again the strongly correlated HF regime and attendant issues of scaling/universality (that play a key role in comparing to experiment), the paper being organised as follows. The model and a bare bones description of background theory is introduced in section 2, together with preliminary consideration of transport/optics. Results for the thermal evolution of single-particle dynamics and scattering rates, and the connection between the two, are given in section 3. The d.c. resistivity is considered in section 4, with particular emphasis in this

context on the crossover from the low- $\tilde{T} = T/\omega_L$ coherent Fermi liquid to the high- \tilde{T} incoherent regime, and explicit connection to single-impurity scaling behaviour. Optical conductivities on all relevant ω - and T -scales are investigated in section 5; and the paper concludes with a brief summary.

2. Model and theory

The Hamiltonian for the PAM is given by $\hat{H} = \hat{H}_c + \hat{H}_f + \hat{H}_{hyb}$:

$$\begin{aligned} \hat{H} = & \epsilon_c \sum_{i,\sigma} c_{i\sigma}^\dagger c_{i\sigma} - t \sum_{(i,j),\sigma} c_{i\sigma}^\dagger c_{j\sigma} + \sum_{i,\sigma} \left(\epsilon_f + \frac{U}{2} f_{i-\sigma}^\dagger f_{i-\sigma} \right) f_{i\sigma}^\dagger f_{i\sigma} \\ & + V \sum_{i,\sigma} (f_{i\sigma}^\dagger c_{i\sigma} + \text{h.c.}) \end{aligned} \quad (2.1)$$

The first two terms represent the uncorrelated conduction (c) band, \hat{H}_c ($\equiv \sum_{\mathbf{k},\sigma} (\epsilon_c + \epsilon_{\mathbf{k}}) c_{\mathbf{k}\sigma}^\dagger c_{\mathbf{k}\sigma}$); with c -orbital site energies ϵ_c and nearest-neighbour hopping matrix element $t_{ij} = t$, rescaled as $t \propto t_*/\sqrt{Z_c}$ in the large dimensional limit where the coordination number $Z_c \rightarrow \infty$ [10–13]. The third term describes the correlated f -levels, \hat{H}_f , with site energies ϵ_f and on-site Coulomb repulsion U ; while the final term \hat{H}_{hyb} hybridizes the c - and f -levels locally via the matrix element V , rendering the otherwise localised f -electrons itinerant.

The model is thus characterized by four independent dimensionless parameters, ϵ_c/t_* , V/t_* , U/t_* and ϵ_f/t_* (t_* sets the scale for the width of the free conduction band and is taken as the basic unit of energy, $t_* \equiv 1$). An equivalent and somewhat more convenient set of ‘bare’/material parameters (with $t_* = 1$) is ϵ_c, V, U and η , where $\eta = 1 + 2\epsilon_f/U$. This parameter space is large, and as such encompasses a wide range of physical behaviour for the paramagnetic phases we consider. The system is of course generically metallic, with non-integral f -level and c -band occupancies ($n_f = \sum_{\sigma} \langle f_{i\sigma}^\dagger f_{i\sigma} \rangle$ and $n_c = \sum_{\sigma} \langle c_{i\sigma}^\dagger c_{i\sigma} \rangle$ respectively). That in turn extends from the trivial case of weakly correlated, perturbative behaviour, through intermediate valence to the strongly correlated heavy fermion (HF) regime. It is naturally the latter, characterized by a low-energy coherence scale ω_L , that is of primary interest. The HF (or Kondo lattice) regime corresponds to essentially localised f -electrons, $n_f \rightarrow 1$, but with arbitrary conduction band filling n_c , the latter being controlled by ϵ_c (which determines the centre of gravity of the free ($V = 0$) conduction band relative to the Fermi level). It arises when $\epsilon_f = -|\epsilon_f|$, for $|\epsilon_f|/\Delta_0 \gg 1$ and $(U - |\epsilon_f|)/\Delta_0 \gg 1$ (whence $-1 \ll \eta < 1$); where $\Delta_0 = \pi V^2 d_0^c(0)$, with $d_0^c(\omega)$ the free conduction electron density of states as specified below and $\omega = 0$ the Fermi level. The heavy fermion regime forms our main focus here; intermediate valence behaviour will be discussed in an experimental context in the following paper.

The exception to the above behaviour arises when $n_f + n_c = 2$. Here the system is generically a Kondo insulator (see *eg* [34]), with an indirect gap in both its $T = 0$ single-particle spectrum *and* optical conductivity [33]; the canonical example being the particle-hole symmetric PAM with $\epsilon_c = 0$ and $\epsilon_f = -U/2$, where $n_f = 1 = n_c$ for all

U. Just like its metallic counterpart arising for $n_f + n_c \neq 2$, the Kondo insulator is however a Fermi liquid, evolving continuously with increasing interaction strength from its non-interacting limit (in this case a ‘hybridization gap insulator’ [43]). As such, the Kondo insulating state is obtained simply as a particular limit of the underlying theory.

2.1. Background theory

A knowledge of local single-particle dynamics and their thermal evolution is well known to be sufficient within DMFT [10–13] to determine transport properties (see section 2.2 below). Our initial focus is thus on the local retarded Green functions $G_{ii}^f(\omega) (\leftrightarrow -i\theta(t)\langle\{f_{i\sigma}(t), f_{i\sigma}^\dagger\}\rangle)$ and likewise $G_{ii}^c(\omega)$ for the c -levels, with corresponding spectra $D_{ii}^\nu(\omega) = -\frac{1}{\pi}\text{Im} G_{ii}^\nu(\omega)$ (and $\nu = c$ or f).

Some brief comments on the free conduction band are first required ($V = 0$ in equation (2.1), where the c - and f -subsystems decouple); specified by the local propagator $g_0^c(\omega)$ with corresponding density of states (dos) $d_0^c(\omega)$. This is given by

$$g_0^c(\omega) = H(\omega^+ - \epsilon_c) \quad (2.2a)$$

$$= \frac{1}{\omega^+ - \epsilon_c - S_0(\omega)} \quad (2.2b)$$

with $\omega^+ = \omega + i0^+$, where for arbitrary complex z

$$H(z) = \int_{-\infty}^{+\infty} d\epsilon \frac{\rho_0(\epsilon)}{z - \epsilon} \quad (2.3)$$

denotes the Hilbert transform with respect to $\rho_0(\epsilon)$; such that from equation (2.2a), $d_0^c(\omega) = \rho_0(\omega - \epsilon_c)$ corresponds simply to a rigid shift of $\rho_0(\omega)$ by ϵ_c . Equation (2.2b) defines the Feenberg self-energy $S_0(\omega)$ [45, 46] as used below, with $S_0(\omega) \equiv S[g_0^c]$ alone (since $g_0^c = H(S + 1/g_0^c)$ from equations (2.2)). The free conduction band is thus determined by the non-interacting dos $\rho_0(\epsilon)$ which, modulo the rigid ϵ_c -shift, reflects the underlying host bandstructure, $\rho_0(\epsilon) \equiv N^{-1} \sum_{\mathbf{k}} \delta(\epsilon - \epsilon_{\mathbf{k}})$. While the formalism below holds for an arbitrary $\rho_0(\epsilon)$, explicit results will later be given for the hypercubic lattice (HCL), for which within DMFT [10–13] $\rho_0(\epsilon) = \pi^{-1/2} \exp(-\epsilon^2)$ is an unbounded Gaussian; and the Bethe lattice (BL), with compact spectrum $\rho_0(\epsilon) = (2/\pi)(1 - \epsilon^2)^{1/2}$ for $|\epsilon| \leq 1$ [10–13]. The HCL will in fact be the primary case, because the Bloch states characteristic of it ultimately underlie the lattice coherence inherent to low-temperature metallic HF behaviour.

The major simplifying feature of DMFT is that the self-energy becomes momentum-independent and hence site-diagonal [10–13]; and since we are interested in the homogeneous paramagnetic phase, the local Green functions $G_{ii}^\nu(\omega) \equiv G^\nu(\omega)$ ($\nu = c, f$) are also site-independent. Straightforward application of Feenberg renormalized perturbation theory [45, 46], then gives the $G^\nu(\omega)$ as

$$G^c(\omega) = \frac{1}{\omega^+ - \epsilon_c - S(\omega) - \frac{V^2}{\omega^+ - \epsilon_f - \Sigma_f(\omega; T)}} \quad (2.4a)$$

$$G^f(\omega) = \frac{1}{\omega^+ - \epsilon_f - \Sigma_f(\omega; T) - \frac{V^2}{\omega^+ - \epsilon_c - S(\omega)}} \quad (2.4b)$$

$$= \frac{1}{\omega^+ - \epsilon_f - \Sigma_f(\omega; T)} \left[1 + \frac{V^2}{\omega^+ - \epsilon_f - \Sigma_f(\omega; T)} G^c(\omega) \right] \quad (2.4c)$$

where $\Sigma_f(\omega; T)$ is the retarded f -electron self-energy ($\Sigma_f(\omega; T) = \Sigma_f^R(\omega; T) - i\Sigma_f^I(\omega; T)$ such that $\Sigma_f^I(\omega; T) \geq 0$). In equations (2.4), $S(\omega)$ is the Feenberg self-energy for the fully interacting case, with $S(\omega) = S[G^c]$ the *same* functional of $G^c(\omega)$ as it is of g_0^c in the $V = 0$ limit. In consequence, $G^c(\omega)$ is given using equations (2.4a), (2.2), (2.3) as

$$G^c(\omega) = H(\gamma) \quad (2.5a)$$

where $\gamma(\omega; T)$ ($= \gamma_R(\omega; T) + i\gamma_I(\omega; T)$) is given by

$$\gamma(\omega; T) = \omega^+ - \epsilon_c - \frac{V^2}{\omega^+ - \epsilon_f - \Sigma_f(\omega; T)}. \quad (2.5b)$$

Let us first point up the physical interpretation of equations (2.4), (2.5). $G^c(\omega)$ is a *local* propagator, and as such familiarly expressed as $G^c(\omega) = N^{-1} \sum_{\mathbf{k}} G^c(\epsilon_{\mathbf{k}}; \omega)$; with the $\epsilon_{\mathbf{k}}$ -resolved conduction electron propagator $G^c(\epsilon_{\mathbf{k}}; \omega) = [\omega^+ - \epsilon_c - \epsilon_{\mathbf{k}} - \Sigma_c(\omega; T)]^{-1}$ and the usual conduction electron self-energy $\Sigma_c(\omega; T)$ thus defined. Since $\rho_0(\epsilon) \equiv N^{-1} \sum_{\mathbf{k}} \delta(\epsilon - \epsilon_{\mathbf{k}})$, it follows directly that

$$G^c(\omega) = \int_{-\infty}^{+\infty} d\epsilon \rho_0(\epsilon) G^c(\epsilon; \omega) \quad \equiv \langle G^c(\epsilon; \omega) \rangle_{\epsilon} \quad (2.6)$$

with ($G^c(\epsilon_{\mathbf{k}} = \epsilon; \omega) \equiv G^c(\epsilon; \omega) = [\omega^+ - \epsilon_c - \Sigma_c(\omega; T) - \epsilon]^{-1}$). But equation (2.6) is precisely the form equation (2.5a) (with equation (2.3) for $H(\gamma)$), showing that

$$G^c(\epsilon; \omega) = [\gamma(\omega; T) - \epsilon]^{-1} \quad (2.7)$$

with $\gamma(\omega; T)$ related to the conduction electron self-energy by

$$\gamma(\omega; T) = \omega^+ - \epsilon_c - \Sigma_c(\omega; T); \quad (2.8)$$

and hence (via equation (2.5b)) that $\Sigma_c(\omega; T) = V^2[\omega^+ - \epsilon_f - \Sigma_f(\omega; T)]^{-1}$ in terms of the f -electron self-energy alone (because the f -levels alone are correlated).

For an arbitrary conduction band (specified by $\rho_0(\epsilon)$) equations (2.4), (2.5) are central; for given the self-energy $\Sigma_f(\omega; T)$, and hence $\gamma(\omega; T)$ from equation (2.5b), $G^c(\omega)$ follows directly from the Hilbert transform equation (2.5a), and $G^f(\omega)$ in turn from equation (2.4c). That statement hides however the truly difficult part of the problem: obtaining the self-energy $\Sigma_f(\omega; T)$. This is not merely a calculational issue, e.g. the need to solve the problem iteratively and self-consistently (any credible approximation to $\Sigma_f(\omega; T)$ will in general be a functional of self-consistent propagators). It reflects by contrast the longstanding problem of obtaining an approximate $\Sigma_f(\omega; T)$ that, ideally: (i) Handles non-perturbatively the full range of interaction strengths, from weak coupling (itself accessible by perturbation theory or simple variants thereof [20–23]) all the way to the strongly correlated Kondo lattice regime that is dominated by spin-fluctuation physics and typified by an exponentially small coherence scale ω_L . (ii) Respects the asymptotic dictates of Fermi liquid behaviour on the lowest energy (ω) and/or T scales – on the order of $|\omega| \lesssim \omega_L$ itself – yet can also handle the *full* ω and/or T range; including the non-trivial dynamics that arise on energy scales up to

many multiples of ω_L yet which remain universal (and the existence of which we find to dominate transport and optics), as well as the non-universal energy scales prescribed by the bare material parameters of the problem.

The success of any theory naturally hinges on the inherent approximation to $\Sigma_f(\omega; T)$. In this paper we employ the local moment approach (LMA) [32–34], for it is known to satisfy the above desiderata and to our knowledge is currently the only theory that does. It is based on an underlying two-self-energy description — a natural consequence of the mean-field approach from which it starts, and from which the conventional single self-energy Σ_f follows — together with the concept of *symmetry restoration* that is central to the LMA generally [35–41]. Full details of the LMA for the PAM, including discussion of its physical basis and content, are given in [32–34]. In particular the generic asymmetric PAM (as considered here) is detailed in [34] for $T = 0$; and extension of it to finite- T , required to consider transport and optics, follows the approach of [33] where the particle-hole symmetric PAM appropriate to the case of Kondo insulators was considered. For that reason further discussion of the approach is omitted here. The reader is instead directed to [33, 34] on the PAM, from which appropriate results will be used when required; and to [35–41] for Anderson impurity models *per se* where details of the LMA, including its strengths and limitations in relation to other approaches, are fully discussed.

2.2. Transport and optics

As mentioned above, a knowledge of single-particle dynamics is sufficient within DMFT to determine $\mathbf{q} = 0$ transport properties [10–13]. This arises because the strict absence of vertex corrections in the skeleton expansion for the current-current correlation function means only the lowest-order conductivity bubble survives [47], and a formal result for it is thus readily obtained. Denoting the trace of the conductivity tensor by $\tilde{\sigma}(\omega; T)$ ($\frac{1}{3}$ of which, denoted by $\sigma(\omega; T)$, provides an approximation to the isotropic conductivity of a 3-dimensional system), this may be cast in the form

$$\tilde{\sigma}(\omega; T) = \sigma_0 F(\omega; T) \quad (2.9)$$

with $\sigma_0 = \frac{\pi e^2 a^2}{\hbar} \frac{N}{V} \simeq \frac{\pi e^2}{\hbar a}$ merely an overall scale factor (a is the lattice constant and σ_0 is typically of order $\approx 10^4 - 10^5 \Omega^{-1} \text{cm}^{-1}$). The dimensionless dynamical conductivity $F(\omega; T)$ naturally depends on the lattice type, and for a Bloch decomposable lattice such as the HCL is given (with $t_* = 1$) by [10–13, 33]

$$F_{HCL}(\omega; T) = \frac{1}{\omega} \int_{-\infty}^{\infty} d\omega_1 [f(\omega_1) - f(\omega_1 + \omega)] \langle D^c(\epsilon; \omega_1) D^c(\epsilon; \omega_1 + \omega) \rangle_{\epsilon} \quad (2.10)$$

where $f(\omega) = [e^{\omega/T} + 1]^{-1}$ is the Fermi function. Here (as in equation (2.6)), the notation $\langle A(\epsilon; \omega) \rangle_{\epsilon} \equiv \int_{-\infty}^{\infty} d\epsilon \rho_0(\epsilon) A(\epsilon; \omega)$ denotes an average with respect to the non-interacting conduction band dos $\rho_0(\epsilon)$; and the spectral density $D^c(\epsilon; \omega) = -(1/\pi) \text{Im} G^c(\epsilon; \omega)$ with $G^c(\epsilon; \omega) = [\gamma(\omega; T) - \epsilon]^{-1}$ from equation (2.7). Physically, $\gamma_I(\omega; T)$ ($= \text{Im} \gamma(\omega; T)$) represents the ω -dependent conduction electron scattering rate (inverse scattering time)

arising from electron interactions, $\gamma_I(\omega; T) \equiv 1/\tau(\omega; T)$ ($= -\text{Im}\Sigma_c(\omega; T)$ from equation (2.8)). It is given using equation (2.5b) by

$$\frac{1}{\tau(\omega; T)} = \gamma_I(\omega; T) = \frac{V^2 \Sigma_f^I(\omega; T)}{[\omega - \epsilon_f - \Sigma_f^R(\omega; T)]^2 + [\Sigma_f^I(\omega; T)]^2} \quad (2.11)$$

in terms of the f -electron self-energy; a knowledge of which thus determines the scattering rates (considered explicitly in section 3.1), and in consequence the dynamical conductivity equation (2.10) (noting that $D^c(\epsilon; \omega) = \gamma_I(\omega; T)\pi^{-1}/([\gamma_R(\omega; T) - \epsilon]^2 + [\gamma_I(\omega; T)]^2)$).

Results for $F_{HCL}(\omega; T)$ obtained using the LMA will be considered in sections 4,5. Here we simply point out an exact result, not apparently well known, for the weight of the Drude peak in the $T = 0$ conductivity. At $T = 0$, scattering at the Fermi level is absent since the system is a Fermi liquid, i.e. $\Sigma_f^I(\omega = 0; T = 0) = 0$ and hence $\gamma_I(0; 0) = 0$. The leading low-frequency behaviour of $\Sigma_f^R(\omega; T)$ is given by

$$\Sigma_f^R(\omega; 0) \sim \Sigma_f^R(0; 0) - (\frac{1}{Z} - 1)\omega \quad (2.12)$$

where $Z = [1 - (\partial\Sigma_f^R(\omega; 0)/\partial\omega)_{\omega=0}]^{-1}$ is the usual quasiparticle weight/inverse mass renormalization; hence (from equation (2.5b)) $\gamma_R(0; 0) = -\epsilon_c + V^2/\epsilon_f^*$, where

$$\epsilon_f^* = \epsilon_f + \Sigma_f^R(0; 0) \quad (2.13)$$

is the renormalized f -level energy. A straightforward evaluation of equation (2.10) for $T = 0$ and $\omega \rightarrow 0$ then shows that $F_{HCL}(\omega; T = 0)$ contains a $\delta(\omega)$ Drude ‘peak’ (as it must, reflecting the total absence of Fermi level scattering and a vanishing $T = 0$ resistivity). Denoted by $F_{Drude}(\omega; 0)$, it is given explicitly by

$$F_{Drude}(\omega; 0) = \delta(\omega) \frac{Z\epsilon_f^{*2}}{Z\epsilon_f^{*2} + V^2} \rho_0(-\epsilon_c + \frac{V^2}{\epsilon_f^*}) \quad (2.14a)$$

or equivalently

$$F_{Drude}(\omega; 0) = \delta(\omega) \frac{\omega_L}{\omega_L + \frac{1}{\tilde{\epsilon}_f^*}} \rho_0(-\epsilon_c + \frac{1}{\tilde{\epsilon}_f^*}) \quad (2.14b)$$

where $\tilde{\epsilon}_f^* = \epsilon_f^*/V^2$ and

$$\omega_L = ZV^2. \quad (2.15)$$

Equations (2.14) are exact, and bear comment. In the trivial limit $V = 0$ where (equation(2.1)) the f -levels decouple from the conduction band, the total Drude weight is naturally $d_0^c(\omega = 0)$, the free conduction band dos at the Fermi level (recall $d_0^c(\omega) = \rho_0(\omega - \epsilon_c)$). For any $V \neq 0$, the Luttinger integral theorem requires

$$\frac{1}{2}(n_c + n_f) = \int_{-\infty}^{-\epsilon_c + 1/\tilde{\epsilon}_f^*} \rho_0(\epsilon) d\epsilon + \theta(-\tilde{\epsilon}_f^*) \quad (2.16)$$

(with $\theta(-\tilde{\epsilon}_f^*)$ merely the unit step function). This again is an exact result, proven in [34]. It holds for *any* interaction U , reflecting the adiabatic continuity to the non-interacting limit that is intrinsic to a Fermi liquid; and shows in general that (any) fixed total filling $n_c + n_f$ determines $-\epsilon_c + 1/\tilde{\epsilon}_f^*$ entering equations (2.14). Of particular interest is

of course the strongly correlated HF regime, where $n_f \rightarrow 1$. Here ω_L in equation (2.15) ($\equiv ZV^2/t_*$ with $t_* = 1$) is the coherence scale: exponentially small in strong coupling (because Z is), it is the *single* low-energy scale in terms of which all properties of the system exhibit universal scaling (as shown in [32–34] and pursued below). In the HF regime, n_c itself is moreover given (see [34]) by

$$\frac{1}{2}n_c = \int_{-\infty}^{-\epsilon_c} \rho_0(\epsilon) d\epsilon \quad (2.17a)$$

showing that ϵ_c and n_c are in essence synonymous, $n_c \equiv n_c(\epsilon_c)$ being determined by ϵ_c alone. Conjoining this with equation (2.16) gives

$$\frac{1}{2}n_f = \int_{-\epsilon_c}^{-\epsilon_c + 1/\tilde{\epsilon}_f^*} \rho_0(\epsilon) d\epsilon + \theta(-\tilde{\epsilon}_f^*) \quad (2.17b)$$

so as $n_f \rightarrow 1$ (the HF regime), $\tilde{\epsilon}_f^* = \tilde{\epsilon}_f^*(\epsilon_c) \equiv \tilde{\epsilon}_f^*(n_c)$ is *also* determined by ϵ_c alone, and is typically of order unity. It is this that determines $\tilde{\epsilon}_f^*$ entering equation (2.14b) for $F_{Drude}(\omega; 0)$; showing in turn that the net Drude weight is itself $\propto \omega_L = ZV^2$, and hence exponentially diminished compared to the free conduction band limit.

We add that Kondo insulators, arising generically for $n_f + n_c = 2$ as mentioned earlier, are also encompassed by the above. Using $\int_{-\infty}^{\infty} d\epsilon \rho_0(\epsilon) = 1$, the Luttinger theorem equation (2.16) shows that $n_f + n_c = 2$ arises either for $\tilde{\epsilon}_f^* = 0$ (for an unbounded $\rho_0(\epsilon)$) or for $-\epsilon_c + 1/\tilde{\epsilon}_f^*$ outside the band edges of a compact $\rho_0(\epsilon)$; such that in either case the Drude weight in equations (2.14) vanishes, symptomatic of the vanishing $T = 0$ d.c. conductivity characteristic of the Kondo insulating state.

Our focus above has naturally been on the canonical case of a Bloch decomposable lattice. For a Bethe lattice by contrast, $F(\omega; T)$ is given [33] by (*cf* equation (2.10))

$$F_{BL}(\omega; T) = \frac{1}{\omega} \int_{-\infty}^{\infty} d\omega_1 [f(\omega_1) - f(\omega_1 + \omega)] D^c(\omega_1) D^c(\omega_1 + \omega) \quad (2.18)$$

where $D^c(\omega)$ ($\equiv \langle D^c(\epsilon; \omega) \rangle_\epsilon$) is the local conduction band spectrum. In particular the d.c. conductivity at $T = 0$ follows as $F_{BL}(0; 0) = [D^c(0)]^2$; which, using $\Sigma_f^I(0; 0) = 0$ together with equations (2.2a), (2.5), (2.12), is given by

$$F_{BL}(0; 0) = [\rho_0(-\epsilon_c + \frac{1}{\tilde{\epsilon}_f^*})]^2. \quad (2.19)$$

In contrast to equations (2.14) there is thus no Drude $\delta(\omega)$ -peak and the $T = 0$ d.c. resistivity is in general finite, reflecting of course that the underlying one-particle states of the BL are not coherent Bloch states. Hence, aside from the case of Kondo insulators where the BL (like the HCL) does capture the vanishing $T = 0$ d.c. conductivity and indirect-gapped optics characteristic of the insulator [33], the ‘joint density of states’ type formula equation (2.19) should not be taken seriously when considering transport/optics of real materials on sufficiently low T and/or ω scales (as discussed further in section 4).

3. Single-particle dynamics

We turn now to LMA results for single-particle dynamics at finite- T . Our natural focus will be the strong coupling Kondo lattice regime (where $n_f \rightarrow 1$), characterized by the low-energy lattice scale $\omega_L = ZV^2$. This scale is of course a complicated function of the bare/material parameters, $\omega_L \equiv \omega_L(\epsilon_c, U, V^2, \eta)$ (detailed LMA results for it are given in [34], and NRG results in [15]). That dependence is however a subsidiary issue in comparison to the fact that, because ω_L becomes exponentially small in strong coupling, physical properties exhibit scaling in terms of it; i.e. depend universally on ω/ω_L , independently of the interaction strength.

Universality in strong coupling single-particle dynamics at $T = 0$ has been considered in [34] for the generic PAM; the essential findings of which are first reprised for use below. (i) Both the c -electron spectrum $D^c(\omega)$ ($\equiv D^c(\omega)/t_*$ with $t_* = 1$) and the f -electron spectrum $\pi\Delta_0 D^f(\omega)$ (with $\Delta_0 = \pi V^2 \rho_0(-\epsilon_c)$ introduced in section 2), exhibit universal scaling as a function of $\tilde{\omega} = \omega/\omega_L$ in a manner that is *independent* of both the interaction strength U and hybridization matrix element V . (ii) That scaling depends in general only on ϵ_c (or equivalently the conduction band filling n_c , see equation (2.17a)) which embodies the conduction band asymmetry; and on $\eta \equiv 1 - 2|\epsilon_f|/U$ reflecting the f -level asymmetry. More specifically, (iii) in the coherent Fermi liquid regime arising for $|\tilde{\omega}| \lesssim 1$, the f -scaling spectra depend only on ϵ_c and are in fact independent of η as well as U and V . In this low- $\tilde{\omega}$ regime the scaling spectra amount in essence to the quasiparticle behaviour (equations (3.11) of [34]) required by the asymptotic dictates of low-energy Fermi liquid theory. (iv) For $|\tilde{\omega}| \gg 1$ by contrast the f -scaling spectra depend on the f -level asymmetry η (albeit rather weakly), but are now independent of ϵ_c and indeed also of the lattice type; and the spectrum contains a long, logarithmically slowly decaying spectral tail. (v) The latter behaviour, which sets in progressively for $|\tilde{\omega}| \gtrsim 1$, reflects in turn the crossover to incoherent effective single-impurity physics that one expects to arise for sufficiently high ω (and/or T): for $|\tilde{\omega}| \gg 1$ the *scaling form* of the f -spectrum is found to be precisely that of an Anderson impurity model (AIM). With increasing $\tilde{\omega}$, dynamics thus cross over from the low-energy quasiparticle behaviour symptomatic of the lattice coherent Fermi liquid state to single-impurity Kondo scaling physics at high $\tilde{\omega}$ (and that this crossover occurs in a single ω/ω_L scaling regime is thus incompatible with the occurrence of ‘two-scale exhaustion’ [44] as explained in [34]).

Figure 1 summarises representative results for $T = 0$ scaling dynamics (irrelevant non-universal energy scales such as U , t_* ($\equiv 1$) or Δ_0 are of course projected out in scaling spectra [32–34]). The main figure shows f/c scaling spectra for the HCL as functions of the scaled frequency $\tilde{\omega} = \omega/\omega_L$, for $\eta = 0$ with $\epsilon_c = 0$ (dashed, and $n_c = 1$) and 0.3 (solid, with $n_c \simeq 0.68$). The $\epsilon_c = 0$ example corresponds to the particle-hole (p-h) symmetric Kondo insulator, whose spectra are thus gapped at the Fermi level $\tilde{\omega} = 0$ (with $\omega_L = ZV^2$ here corresponding to the insulating gap scale [32, 33]). For the asymmetric conduction band $\epsilon_c = 0.3$ by contrast, the gap (which is well developed in strong coupling [34]) moves above the Fermi level; and a sharp lattice-Kondo resonance

symptomatic of the HF metal, straddling the Fermi level and of width $\propto \omega_L$, takes its place in the f -spectra. The inset shows the f -spectra on a much larger $\tilde{\omega}$ scale; displaying the ϵ_c -independence of the slow logarithmic tails [34] and reflecting the crossover to effective single-impurity behaviour (which we emphasise arises whether the system is a HF metal or a Kondo insulator).

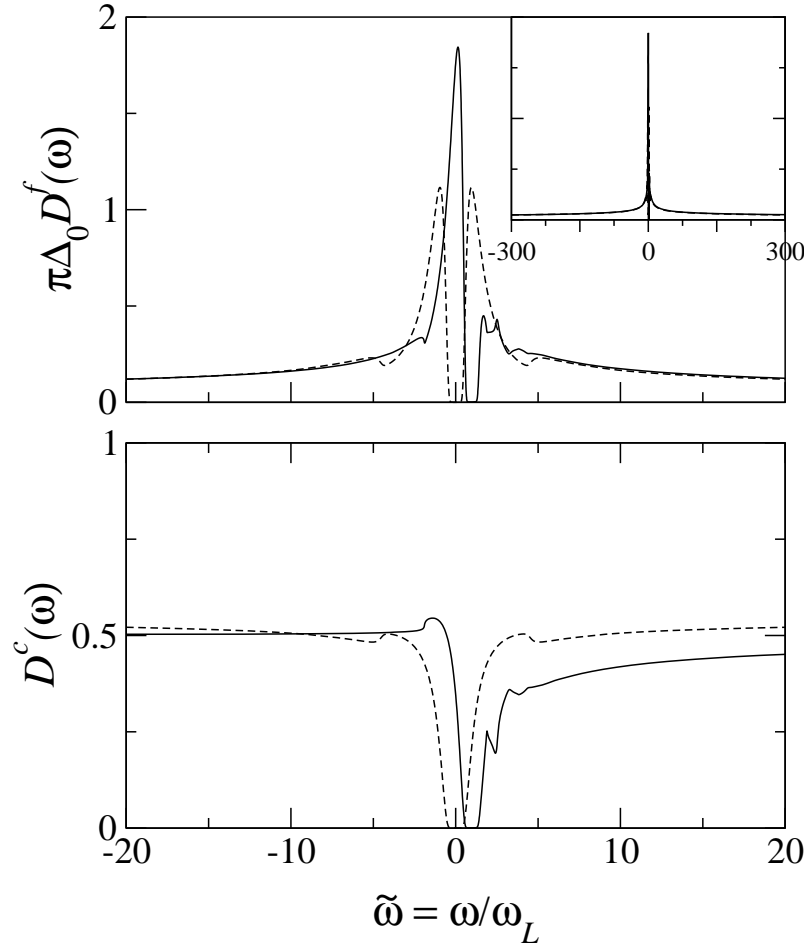


Figure 1. $T = 0$ scaling spectra $\pi\Delta_0 D^f(\omega)$ and $D^c(\omega)$ vs $\tilde{\omega} = \omega/\omega_L$ for the HCL, with $\eta = 0$ and $\epsilon_c = 0$ (dashed), 0.3 (solid). The inset shows the f -spectra on an enlarged $\tilde{\omega}$ scale; showing that the spectral tails are common, independent of ϵ_c .

At finite temperatures, what one expects for the strong coupling scaling spectra is clear: they should now depend universally on $\tilde{\omega} = \omega/\omega_L$ and $\tilde{T} = T/\omega_L$. That this arises correctly within the present LMA is shown in figure 2. For a fixed $\tilde{T} = 2$, the f - and c -spectra are shown for progressively increasing interaction strengths $U = 5.1, 6.1$ and 6.6 with $V^2 = 0.2$; for $\epsilon_c = 0.3$ and $\eta = 0$ (corresponding results for the p-h symmetric limit have been obtained in [33]). The inset shows the f -spectra on an absolute scale (vs ω/t_*), where the exponential reduction of the ω_L -scale with increasing U is clearly seen from the change in the width of the resonance. The main figures by contrast show the spectra as functions of $\tilde{\omega}$, from which the U -independent scaling collapse is

evident; repeating the calculations with different V^2 likewise shows the scaling to be independent of V . This behaviour is not of course confined to the chosen \tilde{T} , and figure 3 shows the resultant LMA scaling spectra for a range of \tilde{T} (again for the representative $\epsilon_c = 0.3, \eta = 0$).

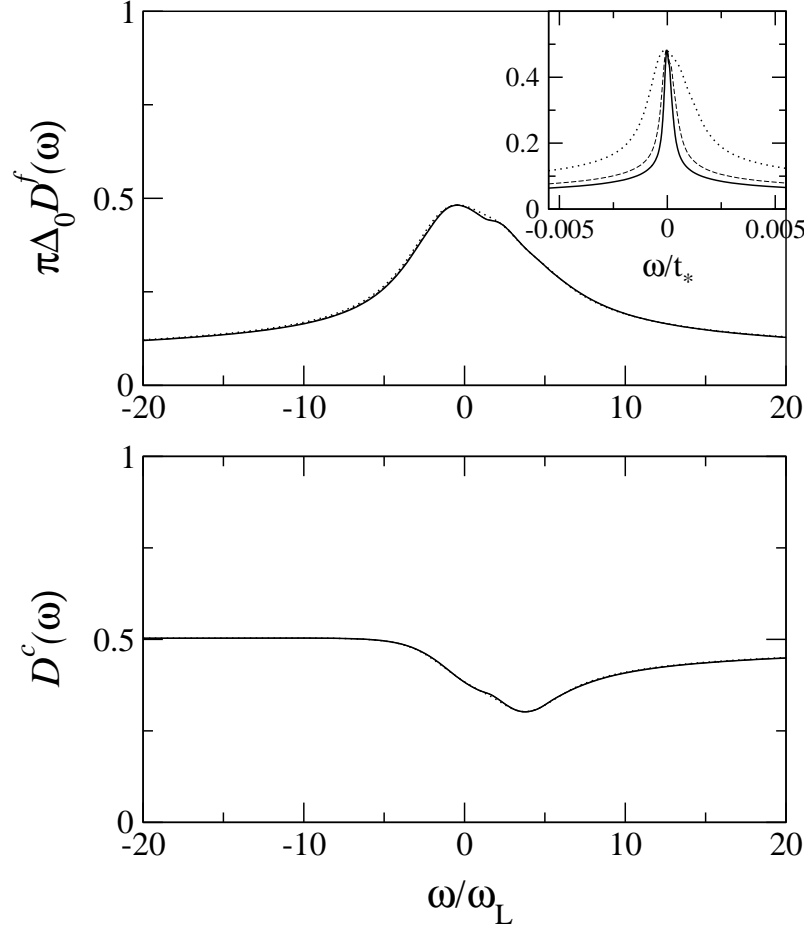


Figure 2. $\pi\Delta_0 D^f(\omega)$ and $D^c(\omega)$ vs ω/ω_L for the HCL at a fixed $\tilde{T} = T/\omega_L = 2$, showing scaling collapse with increasing interaction $U = 5.1$ (dotted), 6.1 (dashed) and 6.6 (solid); for $\eta = 0$ and $\epsilon_c = 0.3$. The inset shows the f -spectra on an absolute scale, vs ω/t_* .

Figures 3 and 2 show clearly the thermal broadening and ultimate collapse of the f -resonance with increasing \tilde{T} ; which is naturally accompanied by a redistribution of spectral weight leading to infilling of the ($\omega > 0$) spectral gap seen in figure 1 for $T = 0$. In fact by $\tilde{T} \sim 1$ this gap is already obliterated, and the lattice Kondo resonance also significantly eroded. This behaviour is typical of the metallic HF state. By contrast, corresponding results for the p-h symmetric Kondo insulator ($\epsilon_c = 0 = \eta$) are shown in figure 4 of [33]. In that case the insulating gap at the Fermi level fills up with increasing temperature, and the Fermi level $D^f(\omega = 0)$ in particular increases monotonically with increasing temperature; in contrast to the the asymmetric HF spectra shown above where $D^f(0)$ diminishes with \tilde{T} .

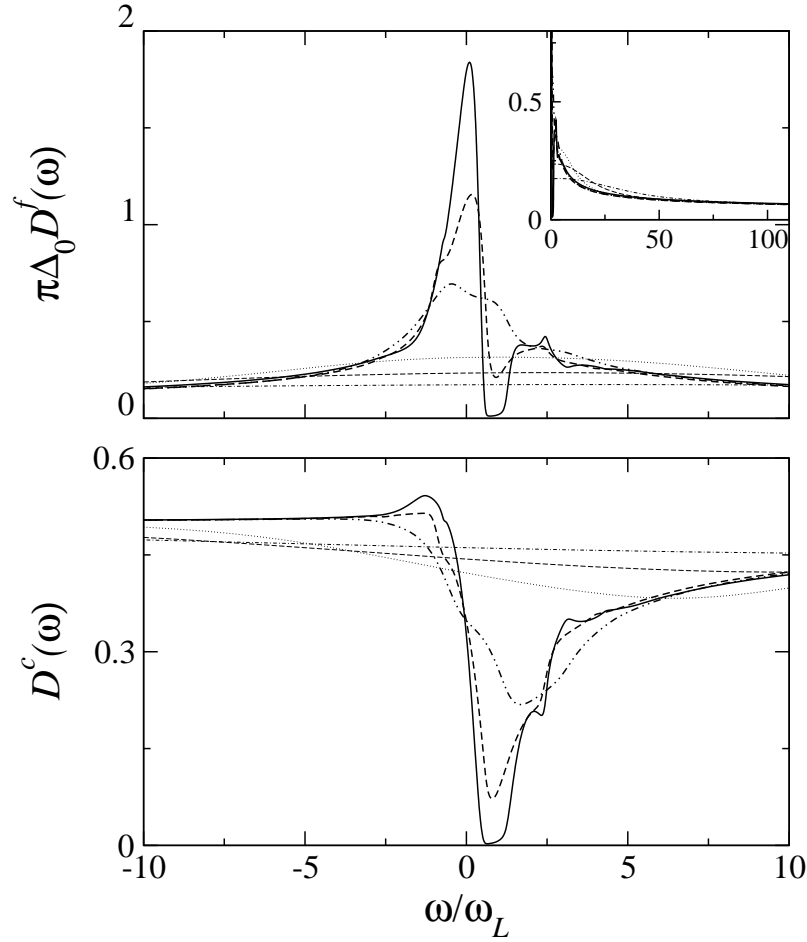


Figure 3. Thermal evolution of HCL scaling spectra $\pi\Delta_0 D^f(\omega)$ and $D^c(\omega)$ vs $\tilde{\omega} = \omega/\omega_L$ for $\epsilon_c = 0.3, \eta = 0$ and temperatures $\tilde{T} = 0.2$ (solid), 0.5 (short-dashed), 1 (double point-dash), 5 (dotted), 10 (long dash) and 20 (point-dash). Inset shows the f -spectra on an enlarged $\tilde{\omega}$ scale.

Two further points regarding figure 3 should be noted. First, the thermal evolution of the f - and c -spectra differ somewhat in terms of the persistence of a pseudogap – the f -spectrum shows no sign of the gap by $\tilde{T} = 1$, while a weak pseudogap structure persists in the c -spectrum up to $\tilde{T} \simeq 5$; this reflects the rapid spread of spectral weight caused by the meltdown of the sharp resonance in the f -spectra, of which there is no counterpart in the c -spectra. Second, the inset to figure 3 shows the f -spectra on an enlarged frequency scale out to $\tilde{\omega} \simeq 100$, from which it is seen that the high frequency behaviour of the finite- \tilde{T} scaling spectra coincide with that for $T = 0$. This is physically natural, since one expects the dominant influence of temperature to be confined to frequencies $|\tilde{\omega}| \lesssim \tilde{T}$. The corollary of course is that non-universal frequencies are affected only on non-universal, and thus in general physically irrelevant, temperature scales (as shown in figure 5 of [33] for the p-h symmetric case).

3.1. Scattering rates

We consider now the scattering rates $\tau^{-1}(\omega; T)$ that underlie the evolution of the conductivity, and are given explicitly in terms of the f -electron self-energy by equation (2.11). Since the system is a Fermi liquid with $\Sigma_f^I(\omega; T = 0) \stackrel{\omega \rightarrow 0}{\sim} \mathcal{O}(\omega^2)$, at $T = 0$ there is of course no scattering at the Fermi level, $\tau^{-1}(0; 0) = 0$. The low frequency behaviour of the $T = 0$ scattering rate can be understood qualitatively by using the low- ω expansion of $\Sigma_f^R(\omega; 0)$ (equation (2.12)) and simply neglecting the imaginary part $\Sigma_f^I(\omega; T)$; leading to

$$\tau^{-1}(\omega; T = 0) \approx \pi \delta(\tilde{\omega} - \tilde{\epsilon}_f^*) \quad (3.1)$$

with $\tilde{\epsilon}_f^* = (\epsilon_f + \Sigma_f(0))/V^2$ the renormalized level. Restoring the small but strictly non-vanishing $\Sigma_f^I(\tilde{\omega} \simeq \tilde{\epsilon}_f^*; T = 0)$ naturally implies a narrow resonance centred on $\tilde{\omega} \simeq \tilde{\epsilon}_f^*$ instead of a pure δ -function. At finite temperature, we likewise expect the scattering rate to increase from zero in the neighbourhood of the Fermi level, reflecting the finite- T contribution to $\Sigma_f^I(\omega \simeq 0; T)$; and that this will simultaneously lead to further, thermal broadening of the resonance at $\tilde{\epsilon}_f^*$.

The above picture is corroborated by LMA results as shown in figure 4, displaying the $\tilde{\omega} = \omega/\omega_L$ dependence of $\tau^{-1}(\omega; T)$ (in units of $t_* \equiv 1$) arising in strong coupling for $\epsilon_c = 0.3$ and $\eta = 0$, for a range of temperatures $\tilde{T} = T/\omega_L$ between 0 and 20. In this case the renormalized level is found to be $\tilde{\epsilon}_f^* \simeq 1$, precisely where $\tau^{-1}(\omega; T = 0)$ has a narrow resonance. With increasing temperature the resonance is indeed seen to broaden and decrease in intensity; and we reiterate that this occurs for temperatures T set by the scale ω_L – the sole low-energy scale characteristic of the problem in strong coupling. Excepting the lowest \tilde{T} we also note that scattering rates in the vicinity of the Fermi level are on the order of 0.1 – 1 of the bandwidth t_* , values some two or so orders of magnitude higher than for conventional clean metals (and indicative of the higher d.c. resistivities that are typical of heavy fermion materials [1]). Neither is this behaviour confined to a narrow \tilde{T} regime since even for $\tilde{T} \gg 1$ the scattering rates decay very slowly with \tilde{T} ; the Fermi level scattering rate for example is readily shown to decay as $\tau^{-1}(0; T) \propto 1/\ln^2(\tilde{T})$.

The scattering rates are also related to the f -electron scaling spectra considered above. For the Kondo insulating p-h symmetric PAM, it was shown in [33] that the dimensionless scattering rate defined as

$$\frac{1}{\tilde{\tau}(\omega; T)} = \frac{\pi \rho_0(-\epsilon_c)}{\tau(\omega; T)} \equiv \tilde{\gamma}_I(\omega; T) \quad (3.2)$$

coincides asymptotically with the f -spectral function, specifically

$$\frac{1}{\tilde{\tau}(\omega; T)} \sim \pi \Delta_0 D^f(\omega) \quad (3.3)$$

in the regime $|\tilde{\omega}| \gg 1$ for any \tilde{T} (the spectral ‘tails’), and for all $|\tilde{\omega}|$ for sufficiently large $\tilde{T} \gg 1$. Equation (3.3) is in fact readily shown to be quite general, and not dependent on p-h symmetry. That it holds for HF metals embodied in the asymmetric PAM is

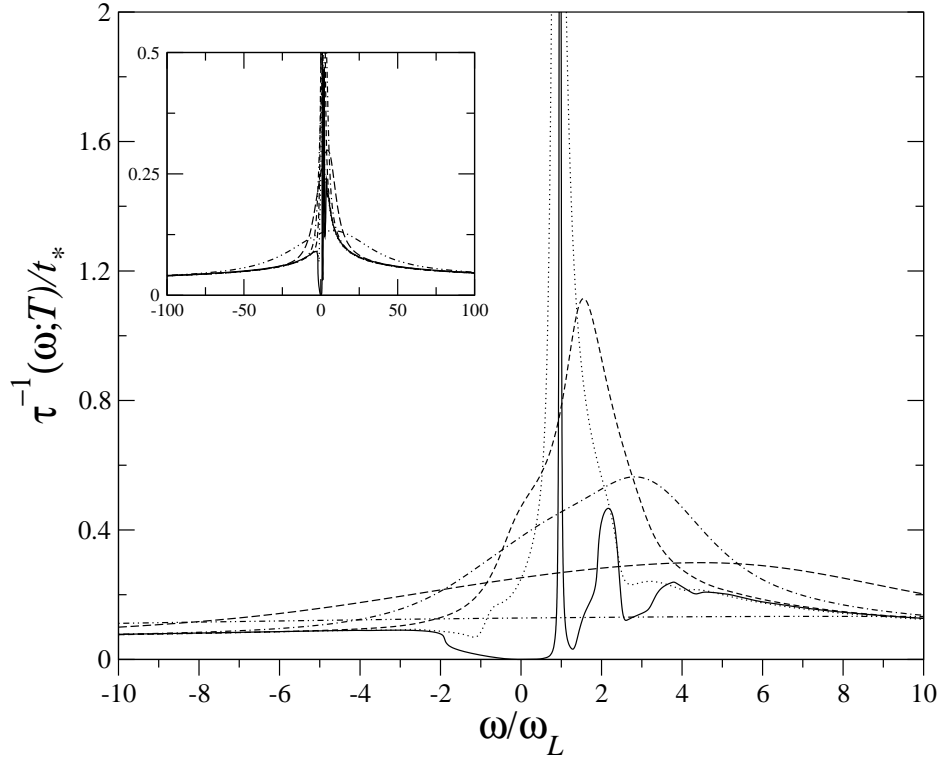


Figure 4. Thermal evolution of the strong coupling scattering rate $\tau^{-1}(\omega; T)/t_*$ vs ω/ω_L (for the HCL) with $\epsilon_c = 0.3, \eta = 0$; for temperatures $\tilde{T} = 0$ (solid), 0.5 (dotted), 1 (short dash), 2 (point-dash), 5 (long dash) and 20 (double point-dash). Inset: the same on an enlarged $\tilde{\omega}$ scale, showing that the high- $\tilde{\omega}$ behaviour coincides with that for $T = 0$.

illustrated in figure 5, where for $\epsilon_c = 0.3$ and $\eta = 0$ the strong coupling $\tilde{\tau}^{-1}(\omega; T)$ and $\pi\Delta_0 D^f(\omega)$ vs $\tilde{\omega}$ are compared, for $\tilde{T} = 0$ in the left panel and $\tilde{T} = 2$ and 10 in the right panel. The high-frequency behaviour of the scaling spectrum $\pi\Delta_0 D^f(\omega)$ is itself known, being given (here for $\eta = 0$ explicitly) by [34]

$$\pi\Delta_0 D^f(\omega) \stackrel{|\tilde{\omega}| \gg 1}{\sim} \frac{1}{2} \left(\frac{1}{\left[\frac{4}{\pi} \ln(a|\tilde{\omega}|)\right]^2 + 1} + \frac{5}{\left[\frac{4}{\pi} \ln(a|\tilde{\omega}|)\right]^2 + 25} \right) \quad (3.4)$$

with a a pure constant $\mathcal{O}(1)$. These slowly decaying logarithmic tails are evident in figure 5, and as mentioned in section 3 embody the connection to effective incoherent single-impurity physics on high energy scales. They are independent of the interaction U , local hybridization V , underlying conduction band asymmetry ϵ_c , and even of the lattice type; depending, albeit weakly, only on the f -level asymmetry [34].

4. DC transport

The above discussion of scattering rates leads naturally to consideration of transport; beginning with the d.c. limit where (section 2.2) the static conductivity $\sigma(0; T) = \frac{1}{3}\sigma_0 F(0; T)$, with $F(\omega; T)$ given for the hypercubic lattice by equation (2.10). In the

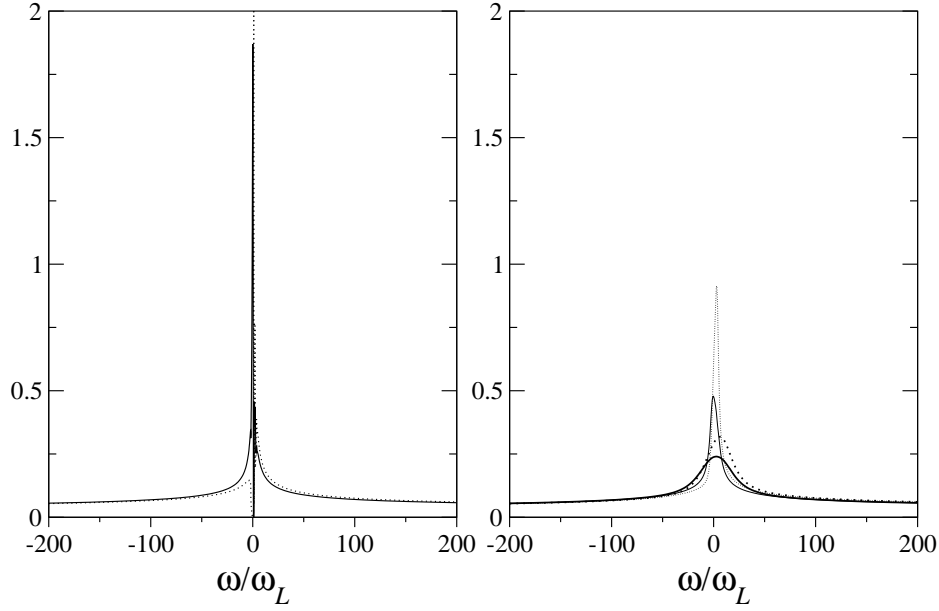


Figure 5. $\pi\Delta_0 D^f(\omega)$ (solid curves) and $\tilde{\tau}^{-1}(\omega; T)$ (dotted) versus $\tilde{\omega}$ (for the HCL with $\epsilon_c = 0.3, \eta = 0$) at $\tilde{T} = 0$ in the left panel; and for $\tilde{T} = 2$ (light curves, solid and dotted) and $\tilde{T} = 10$ (dark curves, solid and dotted) in the right panel.

strong coupling regime we expect static transport to exhibit universal scaling in terms of $\tilde{T} = T/\omega_L$, and our aim here is to understand its thermal evolution across the full \tilde{T} range. Transport on non-universal temperature scales $T \sim \Delta_0$ ($= \pi V^2 \rho_0(-\epsilon_c)$) or $\sim t_*$, will be discussed briefly at the end of the section.

For the p-h symmetric Kondo insulator, LMA results for the \tilde{T} -dependence of the scaling resistivity have been considered in [33] (in this case $\omega_L = ZV^2$ is equivalently the insulating gap scale ‘ Δ_g ’). The $T = 0$ resistivity is naturally infinite reflecting the gapped ground state, the scaling resistivity $\rho(T) = 1/F_{HCL}(0; T)$ has an activated form $\rho(T) \propto \exp(\alpha/\tilde{T})$ for $\tilde{T} \ll 1$ (with α a pure constant $\mathcal{O}(1)$ and hence a ‘transport gap’ of $\alpha\omega_L$); and $\rho(T)$ decreases monotonically with increasing \tilde{T} , tending asymptotically to incoherent single-impurity scaling behaviour ([33] and figures 7,8 below).

For the general case of heavy fermion metals the situation is of course quite different, and what one expects in qualitative terms well known [1, 2]. The $T = 0$ resistivity vanishes, reflecting the absence of Fermi level scattering and the underlying coherence generic to any Bloch decomposable lattice. With increasing temperature $\rho(T)$ increases (initially as $\sim T^2$ for $\tilde{T} \ll 1$ [2, 48]), passes through a maximum at T_{\max} — a classic signature of HF compounds [1–6] — and decreases thereafter in the strong coupling, Kondo lattice regime of interest. Figure 6 shows LMA results for $\rho(T)$ vs \tilde{T} for fixed $\epsilon_c = 0.3, \eta = 0$, and with increasing interaction $U = 4.6, 5.1, 6.1$ and 6.6 for $V^2 = 0.2$. The scaling collapse is clearly evident: while the low-energy scale ω_L itself diminishes exponentially on increasing U , universal scaling of $\rho(T)$ as a function of $\tilde{T} = T/\omega_L$ indeed arises in strong coupling, independent of interaction strength (and likewise readily shown to be V -independent on repeating the calculations varying V^2).

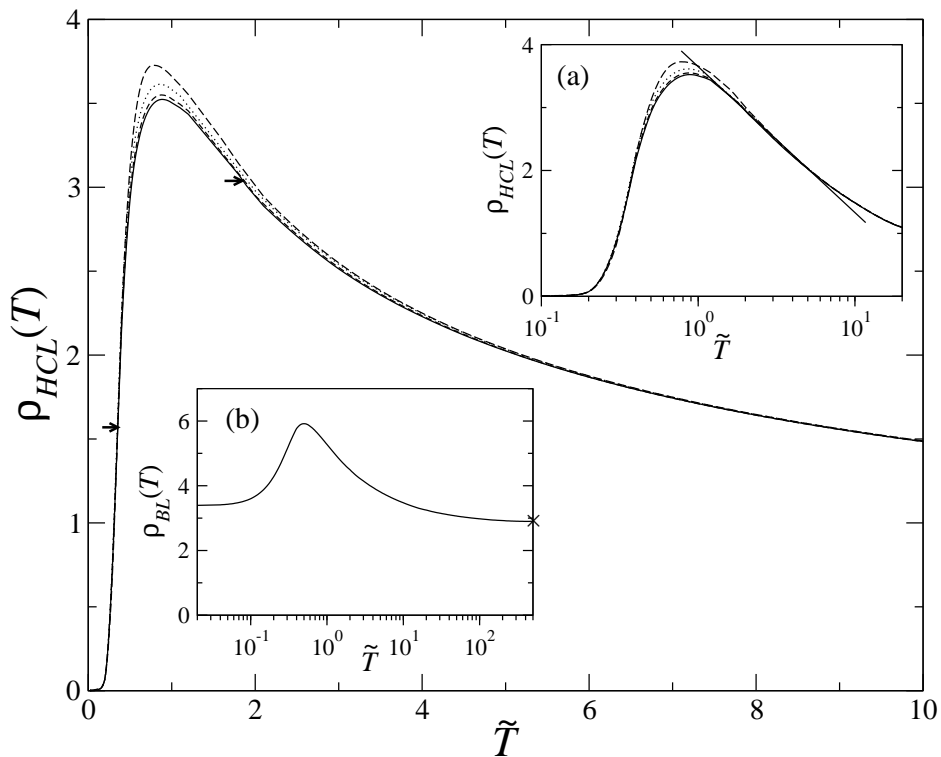


Figure 6. The d.c. resistivity $\rho(T) \equiv 1/F_{HCL}(0; T)$ vs. $\tilde{T} = T/\omega_L$ for $\epsilon_c = 0.3, \eta = 0$ and four interaction strengths: $U = 4.6$ (long dash), 5.1 (dotted), 6.1 (short dash) and 6.6 (solid). Arrows show the inflection points. Inset (a): As in the main figure but on a logarithmic \tilde{T} scale, showing the ‘log-linear’ regime. Inset (b): Scaling resistivity for the Bethe Lattice, for $\epsilon_c = 0.3, \eta = 0$; the cross shows the $T = 0$ resistivity of the free ($V = 0$) conduction band.

This leads us first to comment briefly on the issue of ‘the coherence scale’, characterising the crossover from low-temperature lattice coherent behaviour to high-temperature effective single-impurity behaviour. Experimentally, many such identifications of the low-energy scale are commonly employed. Some groups use T_{\max} at which $\rho(T)$ peaks, others identify the scale via the inflection points ($d^2\rho(T)/dT^2 = 0$, marked by arrows in figure 6), via the leading $\sim T^2$ behaviour of $\rho(T)$ at low- T , or via the onset of the ‘log-linear’ regime [26] (shown in inset (a) to figure 6 and seen in many experimental systems [1–6]); the inverse of the $T \simeq 0$ paramagnetic susceptibility, or the width of the lattice Kondo resonance, are other possibilities. This leads to what at first sight might seem a plethora of low-energy scales. The key point however is that, because physical properties in strong coupling scale universally in terms of *one* low-energy scale, all the above definitions of ‘the coherence scale’ are fundamentally equivalent: all are proportional to ω_L , and hence to each other — in figure 6 for example, the inflection points in $\rho(T)$ lie at $\tilde{T} = T/\omega_L = 0.35$ and 1.85 , and the peak maximum at $\tilde{T} = 0.88$.

As for single-particle dynamics and scattering rates considered in section 3, the \tilde{T} -dependent scaling resistivity is independent of U or V (as above) but depends in general on ϵ_c (reflecting the conduction band asymmetry and determining n_c via

equation (2.17a)) and η (reflecting the f -level asymmetry). To consider this figure 7 shows the resultant scaling resistivities $\rho(T)$ vs \tilde{T} for $\eta = 0$, and a range of different $\epsilon_c = 0, 0.1, 0.3, 0.5$ and 0.6 , corresponding respectively to conduction band fillings $n_c = 1, 0.89, 0.68, 0.49$ and 0.42 . The $\epsilon_c = 0$ example is the Kondo insulator [33], with its characteristic diverging $\rho(T)$ as $\tilde{T} \rightarrow 0$. The others are all HF metals, and exhibit the same qualitative behaviour for all ϵ_c — a positive slope for $\tilde{T} < \tilde{T}_{\max}$, going through the maximum and then decreasing monotonically for $\tilde{T} > \tilde{T}_{\max}$; the coherence peak itself increasing monotonically with ϵ_c , albeit slowly such that $\tilde{T}_{\max} = T_{\max}/\omega_L \sim \mathcal{O}(1)$ for the ϵ_c -range shown. Qualitatively similar behaviour is found on varying the f -level asymmetry η for fixed conduction band asymmetry embodied in ϵ_c , although quantitatively this effect is appreciably less.

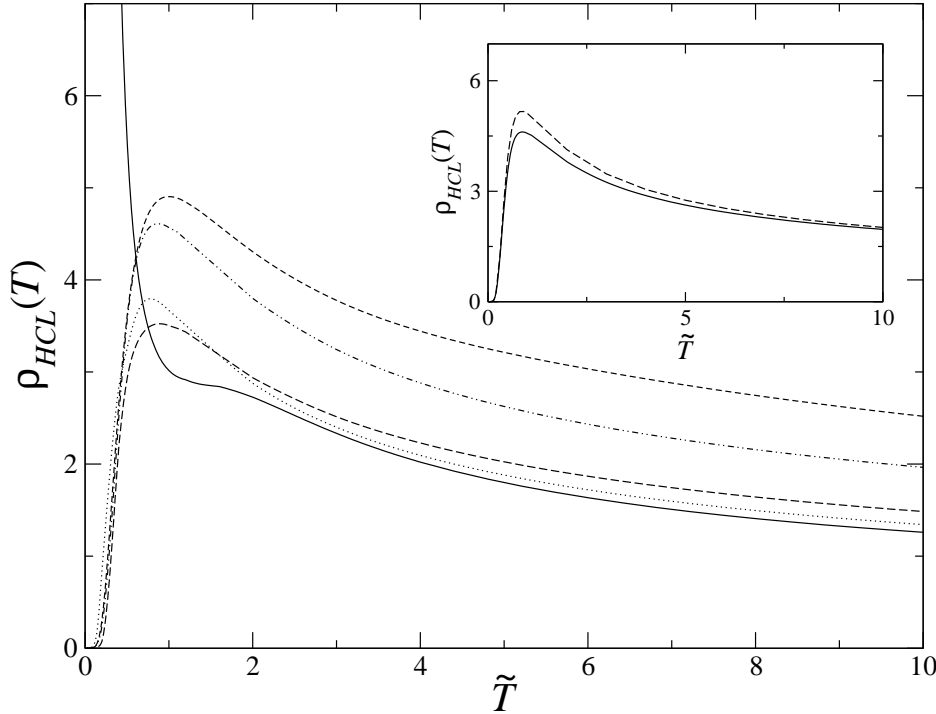


Figure 7. Strong coupling HCL $\rho(T)$ vs. \tilde{T} for $\eta = 0$ and $\epsilon_c = 0$ (solid), 0.1 (dotted), 0.3 (long dash), 0.5 (double point dash) and 0.6 (short dash) Inset: for $\epsilon_c = 0.5$, full result (solid) compared to the approximation equation (4.1) (dashed).

The significant ϵ_c -dependence of $\rho(T) = 1/F_{HCL}(0; T)$ seen in figure 7 for $\tilde{T} \gtrsim \tilde{T}_{\max}$ is intuitively natural: the strong coupling Kondo lattice regime corresponds to $n_f = 1$, but with variable conduction band filling (n_c) controlled by ϵ_c (equation (2.17a)); and on decreasing n_c (increasing ϵ_c) one expects the static conductivity to diminish and hence an increased $\rho(T)$, as found. To understand the ϵ_c -dependence, and in turn to enable connection to incoherent effective single-impurity behaviour at high- \tilde{T} , we first consider an approximate evaluation of $F_{HCL}(0; T)$ (equation (2.10)); in which the energy dependence of the free conduction band dos $d_0^c(\epsilon) = \rho_0(\epsilon - \epsilon_c)$ is neglected, $d_0^c(\epsilon) \simeq d_0^c(0) = \rho_0(-\epsilon_c)$ being replaced by its Fermi level value. Employing this ‘flat

band' approximation in equation (2.10) (where it enters via the $\langle \dots \rangle_\epsilon$ average) leads to

$$F_{HCL}(0; T) \simeq \frac{1}{2}[\rho_0(-\epsilon_c)]^2 \int_{-\infty}^{+\infty} d\omega \frac{-\partial f(\omega)}{\partial \omega} \tilde{\tau}(\omega; T) \quad \equiv \quad \frac{1}{2}[\rho_0(-\epsilon_c)]^2 \langle \tilde{\tau} \rangle \quad (4.1)$$

expressed as a physically intuitive thermal average of the dimensionless scattering time $\tilde{\tau}(\omega; T)$ (equation (3.2)). For Kondo insulators this approximation is qualitatively inadequate at low- \tilde{T} [33], but as illustrated in figure 7 (inset) it is entirely respectable for the HF metals and in particular recovers precisely the high- \tilde{T} asymptotics of $\rho(T)$. As shown in section 3.1, the large $\tilde{\omega}$ and/or \tilde{T} dependence of the reduced scattering rate $\tilde{\tau}^{-1}(\omega; T)$ coincides with the f -spectral function $\pi\Delta_0 D^f(\omega)$ (equation (3.3)); and in section 3 (see also [34]) the latter were shown to have common spectral tails, independently of ϵ_c . This suggests that the primary effect of ϵ_c seen in figure 7 for $\rho(T) = 1/F_{HCL}(0; T)$ is contained in the $[\rho_0(-\epsilon_c)]^2$ of equation (4.1).

That this is so is seen in figure 8 where the results of figure 7 are now shown as $\rho'(T)$ vs \tilde{T} , where

$$\rho'(T) = \frac{\frac{1}{2}[\rho_0(-\epsilon_c)]^2}{F_{HCL}(0; T)}. \quad (4.2)$$

For $\tilde{T} \gtrsim 5$ or so in practice, $\rho'(T)$ is seen in particular to be *independent* of the conduction band filling embodied in ϵ_c ; including we note the Kondo insulator, whose 'high' temperature resistivity is thus seen to be that of a regular heavy fermion metal. Indeed as readily demonstrated, and evident in part from the above discussion, the behaviour seen in figure 8 is barely dependent on the details (ϵ -dependence) of the host bandstructure embodied in $\rho_0(\epsilon)$.

The obvious final question here concerns the high- \tilde{T} form of $\rho'(T)$ for the PAM. To that end we consider the Anderson single-impurity model (AIM), with $\rho_{\text{imp}}(T)$ denoting as usual the change of resistivity due to addition of the impurity to the non-interacting host, and $\rho'_{\text{imp}}(T) = \rho_{\text{imp}}(T)/\rho_{\text{imp}}(0)$. This is given by [2] (*cf* equations (4.1),(4.2))

$$\frac{1}{\rho'_{\text{imp}}(T)} = \int_{-\infty}^{+\infty} d\omega \frac{-\partial f(\omega)}{\partial \omega} \tilde{\tau}_{\text{imp}}(\omega; T) \quad (4.3)$$

with the impurity scattering rate $\tilde{\tau}_{\text{imp}}^{-1}(\omega; T) = \pi\Delta_0 D_{\text{imp}}(\omega; T)$; where $D_{\text{imp}}(\omega; T)$ is the impurity spectral function such that $\pi\Delta_0 D_{\text{imp}}(0; 0) = 1$ follows from the Friedel sum rule [2] in the singly occupied, strong coupling Kondo regime of the AIM. The LMA scaling resistivity $\rho'_{\text{imp}}(T)$ vs \tilde{T} is also shown in figure 8, where $\tilde{T} = T/\omega_K$ and $\omega_K = Z_{\text{imp}}V^2$ is the AIM Kondo scale (with Z_{imp} the impurity quasiparticle weight). From this it is seen that the high- \tilde{T} scaling behaviour of $\rho'(T)$ for the PAM is precisely that of the AIM; in particular the leading $\tilde{T} \gg 1$ behaviour of the LMA $\rho'(T)$ is readily shown analytically to be given by $\rho'(T) \sim 3\pi^2/(16\ln^2(\tilde{T}))$, which is exact in the Kondo limit of the impurity model [2]. This reflects again the crossover in the strong coupling PAM from low-temperature lattice coherent behaviour to incoherent effective single-impurity scaling physics, here in the context of d.c. transport. As for its counterpart in the case of single-particle dynamics [34], we point out (a) that since this connection

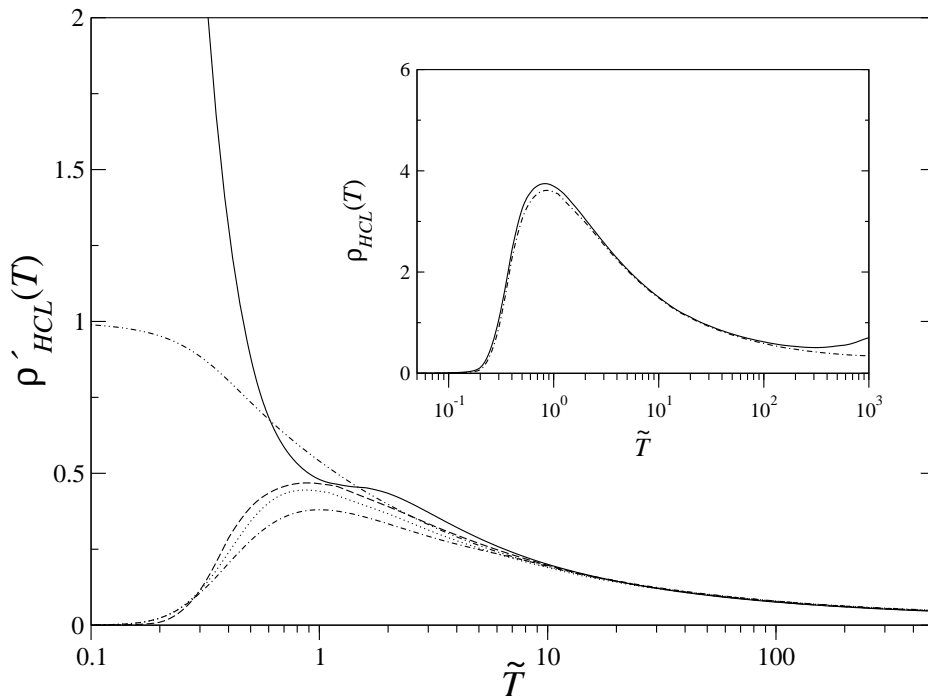


Figure 8. Scaling resistivities $\rho'(T)$ vs. \tilde{T} for $\eta = 0$ and $\epsilon_c = 0$ (solid), 0.3 (long dash), 0.5 (dotted) and 0.6 (point dash); *c.f.* figure 7. $\rho'_{\text{imp}}(T)$ for the single-impurity AIM (equation (4.3)) is also shown (double point dash). For inset, see text.

is established from scaling considerations it is entirely independent of how the scales ω_L and ω_K for the two distinct models (PAM and AIM) depend on the underlying bare/material parameters of the respective problems; and (b) the fact that it arises in the T/ω_L scaling regime precludes a two-scale description of the crossover from lattice-coherent to incoherent effective single-impurity physics.

Our focus above has naturally been on the strong coupling, Kondo lattice regime. We now look briefly at d.c. transport on non-universal scales. What one expects here is that when the temperature is a not insignificant fraction of the hybridization Δ_0 or bandwidth scale $t_*(\equiv 1)$, Kondo screening will be washed out, and hence $\rho(T)$ should cross over from the logarithmically decreasing single-impurity form at $\tilde{T} \gg 1$ (figures 7 and 8) to conventional metallic behaviour $d\rho(T)/dT > 0$ at non-universal temperatures; and thus as such must go through a minimum. That this indeed happens can be seen in the inset to figure 8 where we show $\rho(T) = 1/F_{HCL}(0; T)$ vs $\tilde{T} = T/\omega_L$ for $\epsilon_c = 0.3$, $\eta = 0$, $V^2 = 0.2$ and $U = 4.1$ (solid line) and 5.6 (point-dash). For the lower U example, a minimum is seen at $\tilde{T} = T/\omega_L \sim 300$, which corresponds in ‘absolute’ units (t_*) to a temperature $T \simeq 0.2$ — an appreciable fraction of the hybridization $\Delta_0 \simeq 0.3$. The corresponding minimum does of course exist for the higher U , but is pushed beyond $\tilde{T} = 10^3$ (and to concomitantly lower values of $\rho(T)$); and $\rho(T)$ in this case lies on the universal scaling curve throughout the \tilde{T} -range shown in figure 8.

A final point is worth noting here. For $\tilde{T} \lesssim 10^2$, the $\rho(T)$ vs $\tilde{T} = T/\omega_L$ for the two U ’s shown in figure 8 (inset) are in essence coincident; each lies on the universal

scaling curve. What distinguishes different interaction strengths is of course the location of the minimum, occurring as it does on non-universal temperature scales. No real HF material is however in the universal scaling regime ‘for ever’ — with increasing T the scaling regime will be exited sooner or later. And the temperature for which the experimental $\rho(T)$ is a minimum (once phonon contributions have been subtracted out) can provide valuable information on the interaction strength, as we shall see in action in the following paper.

4.1. Bethe lattice

We have considered almost exclusively the hypercubic lattice, for the obvious reason that its one-particle Bloch states ultimately underlie the low-temperature lattice coherence of the interacting problem. For the Bethe lattice, the strong coupling scaling resistivity $\rho(T) = 1/F_{BL}(0; T)$ (with $F_{BL}(\omega; T)$ from equation (2.18)) is shown *vs* \tilde{T} in inset (b) to figure 6, for $\epsilon_c = 0.3, \eta = 0$. In contrast to its counterpart for the HCL shown in the main figure, the $\tilde{T} = 0$ resistivity is non-vanishing (given by equation (2.19)), reflecting the absence of coherent Bloch states for the BL. Further, the *high*- \tilde{T} asymptote of the BL $\rho(T)$ in the scaling regime is likewise non-zero; being given by the $T = 0$ value of the free ($V = 0$) conduction band resistivity, namely $1/[\rho_0(-\epsilon_c)]^2 = \pi^2/[4(1 - \epsilon_c^2)]$ as marked by a cross in figure 6 inset (and arising for the same physical reasons discussed for Kondo insulators in [33]). The qualitative contrast between $\rho(T)$ for the canonically Bloch decomposable HCL, and that for the BL, illustrates why the latter — more specifically the associated ‘joint density of states’ type formula equation (2.18) for $F(0; T)$ that is not uncommonly employed in the literature — gives a poor caricature of d.c. transport for HF metals in which the lattice coherence is of central importance.

5. Optical conductivity

We turn now to the optical conductivity $\sigma(\omega; T) = \frac{1}{3}\sigma_0 F(\omega; T)$ (with $F_{HCL}(\omega; T)$ given by equation (2.10)). In the strong coupling Kondo lattice regime $F_{HCL}(\omega; T)$ is of course independent of U and V^2 , and a universal function of $\tilde{\omega} = \omega/\omega_L$ and $\tilde{T} = T/\omega_L$ for fixed ϵ_c and η .

LMA results for $F_{HCL}(\omega; T)$ are shown in figure 9, for $\epsilon_c = 0.3$ and $\eta = 0$. The right panel shows the thermal evolution of the optical conductivity (on a linear $\tilde{\omega}$ -scale) for temperatures $\tilde{T} = 0, 0.5, 1, 2, 5$ and 10; while the left panel (on a log-log scale) shows the behaviour for a lower range of temperatures up to $\tilde{T} = 0.5$. The latter in particular illustrates the thermal evolution of the optical Drude peak, which at $T = 0$ consists of an $\omega = 0$ δ -function given by equations (2.14) (with net weight $\propto \omega_L$ in strong coupling). On increasing \tilde{T} from 0 the Drude peak naturally broadens, and is well fit by a Lorentzian up to its half-width or so, after which it decays more slowly in $\tilde{\omega}$. At the lowest \tilde{T} shown the Drude peak is well separated from the ‘optical edge’ in $F_{HCL}(\omega; T)$ seen at $\tilde{\omega} \simeq 2$ (although we add that $F_{HCL}(\omega; T)$ is strictly non-zero for all $\tilde{\omega}$), and with

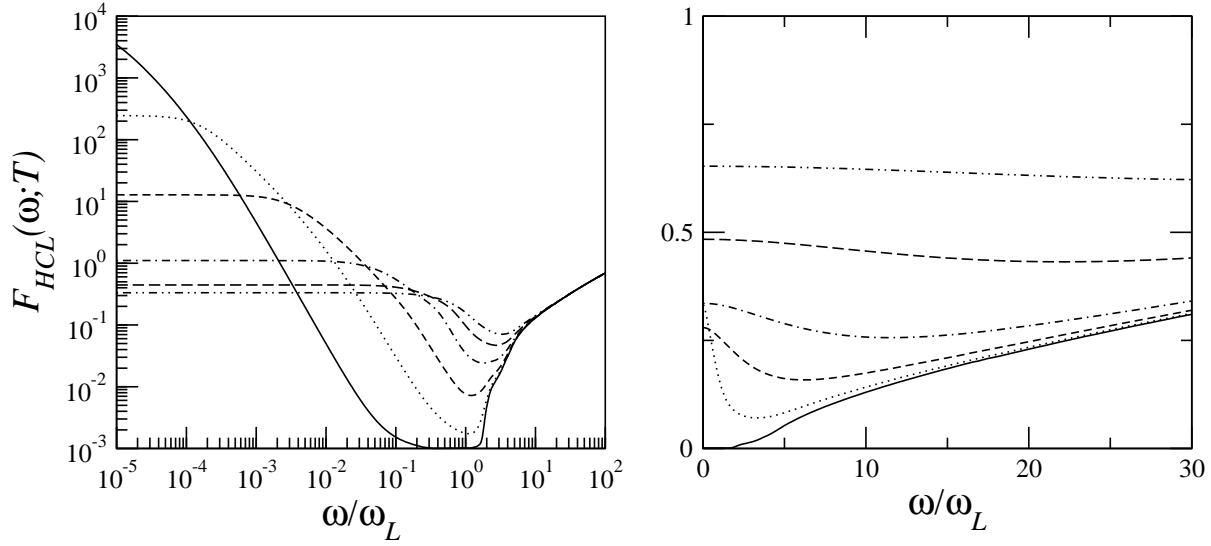


Figure 9. $F_{HCL}(\omega; T)$ vs. $\tilde{\omega} = \omega/\omega_L$ in the Kondo lattice scaling regime for a range of temperatures $\tilde{T} = T/\omega_L$; for $\epsilon_c = 0.3$ and $\eta = 0$. Left panel: On a log-log scale, for $\tilde{T} = 0.02$ (solid), 0.1 (dotted), 0.2 (short dash), 0.3 (point dash), 0.4 (long dash) and 0.5 (double point dash), showing the evolution of the Drude peak. Right panel: On a linear scale, for $\tilde{T} = 0$ (solid), 0.5 (dotted), 1 (short dash), 2 (point dash), 5 (long dash) and 10 (double point dash).

increasing \tilde{T} is seen to persist as an essentially separate entity up to $\tilde{T} \sim 0.1$ or so; after which it is progressively destroyed as expected, merging into an optical pseudogap in the neighbourhood of $\tilde{\omega} \sim 1 - 2$, which is reasonably well filled up by $\tilde{T} \sim 0.5$ and all but gone by $\tilde{T} \sim 2$ (see figure 9, right panel). Similar behaviour is naturally found on varying ϵ_c and/or η . Figure 10 shows in particular the influence of ϵ_c (varying conduction band filling) on the optical pseudogap for a fixed temperature $\tilde{T} = 0.2$, from which it is seen that the pseudogap becomes shallower with increasing ϵ_c .

The above behaviour should be compared to the p-h symmetric Kondo insulator (KI) $\epsilon_c = 0 = \eta$ considered in [33]. In that case the $T = 0$ optical conductivity is characterized by an indirect gap $\Delta_{ind} = 2ZV^2 = 2\omega_L$, and there is of course no $T = 0$ Drude peak. Instead a Drude-like peak in the optical conductivity actually builds up on initially increasing \tilde{T} from zero (see figure 15 of [33]), before being thermally broadened and subsumed into the optical pseudogap. For $\tilde{T} \lesssim 1$ or so the low-frequency optics of the KI are thus very different from those of the HF metal, as expected. But for $\tilde{T} \gtrsim 1$ the optical behaviour of the two is qualitatively similar as shown by comparison of figure 9 (right panel) and its counterpart for the KI, figure 14 of [33]. This too is physically natural, since the infilling of the indirect optical gap on temperature scales $\tilde{T} \sim 1$ means that the KI behaves to all intents and purposes as a HF metal; as seen also in figures 7 or 8 for the static transport.

A second point should be emphasised here, obvious though it is from the preceding discussion: whether for HF metals or Kondo insulators, it is the low-energy scale $\omega_L = ZV^2$ that sets the intrinsic scale for both the ω -dependence of the low-energy

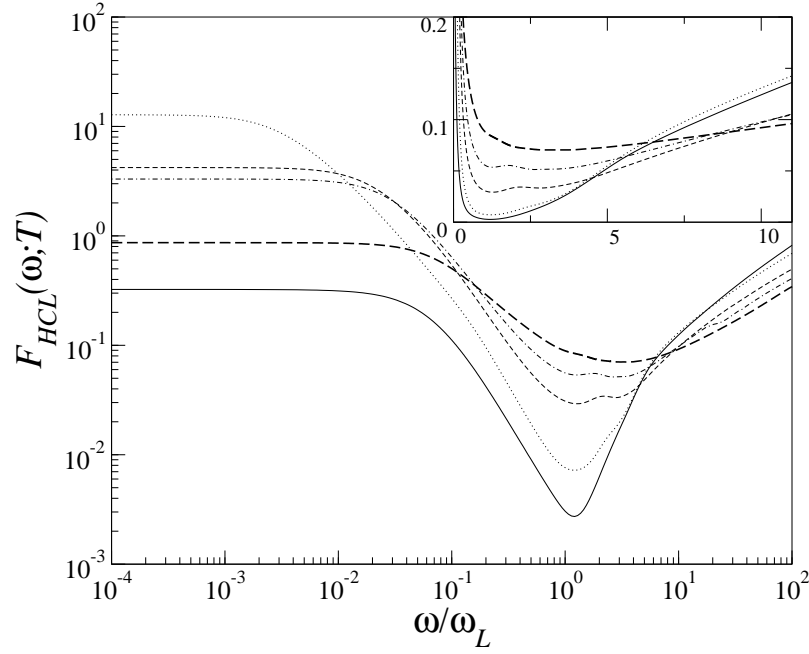


Figure 10. $F_{HCL}(\omega; T)$ vs. $\tilde{\omega}$ for fixed $\tilde{T} = 0.2$ in the Kondo lattice scaling regime for $\eta = 0$ and $\epsilon_c = 0.1$ (solid), 0.3 (dotted), 0.5 (short dash), 0.6 (dot dash) and 0.8 (long dash). Inset: shown on a linear scale.

optical conductivity and its thermal evolution. And in strong coupling that scale is wholly distinct from the optical *direct* gap, Δ_{dir} . The latter arises at its simplest in the commonly employed renormalized band picture (see e.g. [2]), as the minimum direct gap for which optical transitions are allowed. In this effective single-particle description the imaginary part of the f -electron self-energy – and hence all scattering – is neglected entirely, and the corresponding real part $\Sigma_f^R(\omega; 0)$ is replaced by its leading low- ω behaviour equation (2.12) (as also inherent to a slave boson mean-field approximation [2]). The two branches of the renormalized bandstructure, denoted by $\omega_{\pm}(\epsilon)$ with $\epsilon \equiv \epsilon_{\mathbf{k}}$, then follow from the zeros of $[G^c(\epsilon_{\mathbf{k}}; \omega)]^{-1} = [\gamma(\omega) - \epsilon_{\mathbf{k}}]$ (see equation (2.7)) with the approximate $(\gamma(\omega) \equiv) \gamma_R(\omega) \simeq \omega - \epsilon_c - ZV^2[\omega - Z\epsilon_f^*]^{-1}$ from equation (2.5b); and the resultant ϵ -dependent direct gap $\Delta_d(\epsilon) = [\omega_+(\epsilon) - \omega_-(\epsilon)]$ is given by $\Delta_d(\epsilon) = [(\epsilon + \epsilon_c - Z\epsilon_f^*)^2 + 4ZV^2]^{1/2}$ with $\epsilon_f^* = \epsilon_f + \Sigma_f^R(0; 0)$ the usual renormalized level. The minimum direct gap, Δ_{dir} , occurs for $\epsilon + \epsilon_c = Z\epsilon_f^*$ ($\simeq 0$ in strong coupling) and is thus

$$\Delta_{\text{dir}} \simeq 2\sqrt{Z}V. \quad (5.1)$$

The corresponding result for the optical conductivity $F_{HCL}(\omega; T)$ is readily determined from equation (2.10). Denoted by $F_o(\omega; T)$ it is given for $T = 0$ (and all $\omega > 0$) by

$$F_o(\omega; 0) = \frac{\theta(\omega - \Delta_{\text{dir}})}{\sqrt{\omega^2 - \Delta_{\text{dir}}^2}} \frac{\Delta_{\text{dir}}^2}{4\omega^2} \left[d_0^c \left(\epsilon_f^* + \sqrt{\omega^2 - \Delta_{\text{dir}}^2} \right) + d_0^c \left(\epsilon_f^* - \sqrt{\omega^2 - \Delta_{\text{dir}}^2} \right) \right] \quad (5.2)$$

with $d_0^c(\omega) = \rho_0(\omega - \epsilon_c)$ the free conduction band dos and $\theta(x)$ the unit step function; and is thus non-zero only for frequencies $\omega > \Delta_{\text{dir}}$ *above* the direct gap (which result is

also readily shown to hold for *all* temperatures).

Two points should be noted here. First that the low-energy scale $\omega_L = ZV^2$ intrinsic to HFs or KIs is qualitatively distinct from the direct gap Δ_{dir} . In fact since $\Delta_{\text{dir}}/\omega_L \propto 1/\sqrt{\omega_L}$ it follows that in strong coupling where the quasiparticle weight Z and hence ω_L becomes exponentially small, optics on the direct gap scale do not even lie in the $\tilde{\omega} = \omega/\omega_L$ scaling regime; although neither do they occur on truly non-universal scales (because $\Delta_{\text{dir}} \propto \sqrt{Z}$) and in that sense belong to the ‘low-frequency’ optical spectrum. Second, we emphasise the inherent naiveté of interpreting optics in terms of renormalized single-particle interband transitions: it is scattering due to electron interactions that generates *all* the optical density below the direct gap scale. Failure to include such, as in a renormalized band picture — and regardless of how sophisticated the underlying band structure employed in practice — inevitably leads to a qualitatively inadequate description of optics (as illustrated explicitly in figure 11 below). Neither is this situation ameliorated in materials application by the introduction of *ad hoc* ω -dependent broadening factors, for that simply avoids the basic underlying physics.

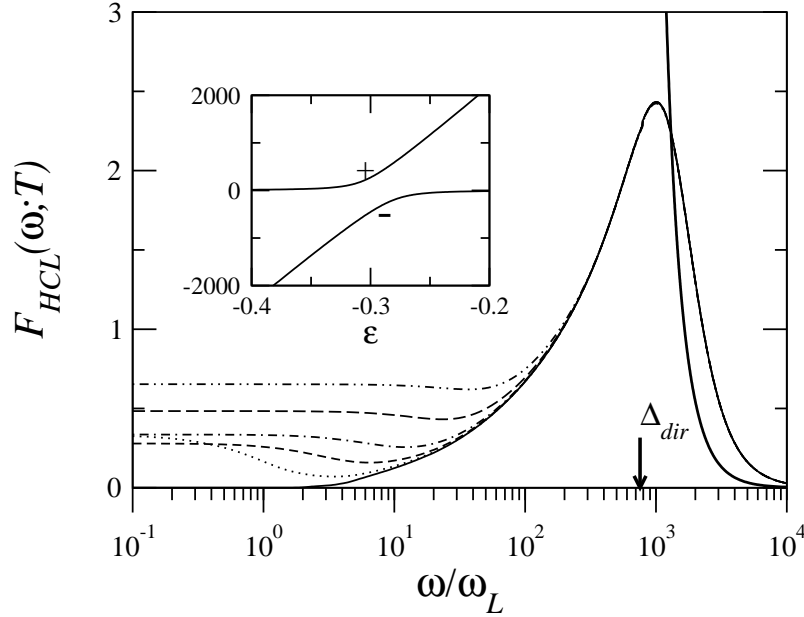


Figure 11. $F_{HCL}(\omega; T)$ vs $\tilde{\omega} = \omega/\omega_L$ on a log scale for $\epsilon_c = 0.3, \eta = 0$ with $U = 6.6$ and $V^2 = 0.2$; and temperatures $\tilde{T} = T/\omega_L = 0$ (solid), 0.5 (dotted), 1 (short dash), 2 (point dash), 5 (long dash) and 10 (double point dash). Comparison is also made to the renormalized band picture equation (5.2) (thick solid line). Inset: renormalized bandstructure $\omega_{\pm}(\epsilon)/\omega_L$ versus the free ($V = 0$) conduction band energies $\epsilon \equiv \epsilon_{\mathbf{k}}$.

LMA results for optics on all frequency scales are given in figure 11, for $\epsilon_c = 0.3, \eta = 0$; where $F_{HCL}(\omega; T)$ is shown vs $\tilde{\omega} = \omega/\omega_L$ on a log scale spanning five orders of magnitude, for the same range of temperatures $\tilde{T} = T/\omega_L$ employed in figure 9 (right panel). To encompass all ω including non-universal energies, the bare parameters U and V^2 must of course be specified, $U = 6.6$ and $V^2 = 0.2$ here being chosen for illustration; although note that the optical conductivity as a function of $\tilde{\omega} = \omega/\omega_L$ remains ‘universal’

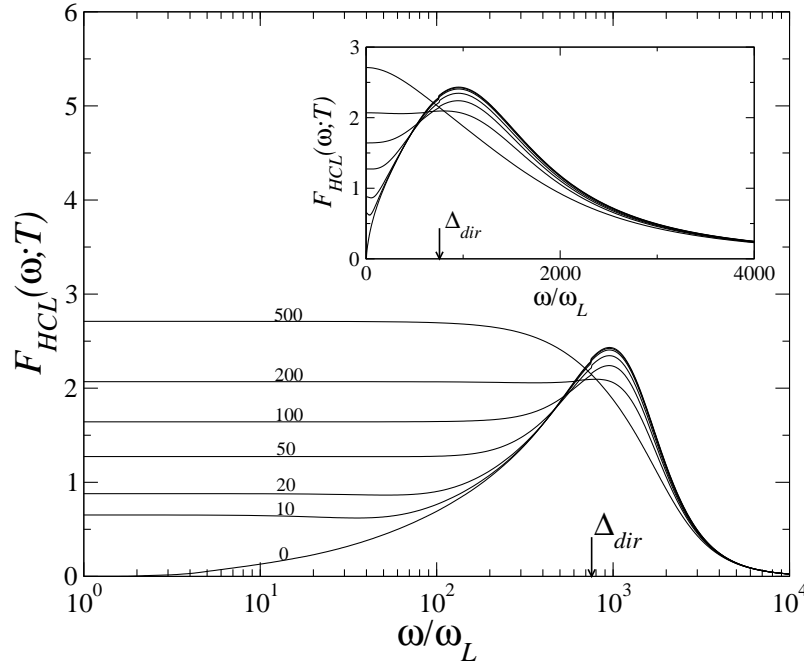


Figure 12. $F_{HCL}(\omega; T)$ vs. $\tilde{\omega} = \omega/\omega_L$ for the same parameters as in figure 11, and temperatures $\tilde{T} = T/\omega_L$ from 0 to $\tilde{T} = 500 \simeq \frac{2}{3}\Delta_{\text{dir}}$ as marked on the figure. Inset: same on a linear scale.

(independent of U or V^2) up to large but finite values of $\tilde{\omega}$ determined by the particular U and V^2 chosen, in this example $\tilde{\omega} \sim 300 - 400$ (a directly analogous situation for the resistivity $\rho(T)$ is shown in the inset to figure 8). The inset to figure 11 shows the renormalized bandstructure $\tilde{\omega}_{\pm}(\epsilon) = \omega_{\pm}(\epsilon)/\omega_L$ vs the free conduction band energy ϵ ; determined as above from solution of $\gamma_R(\omega) = \epsilon$ (with $\gamma_R(\omega)$ the full $\text{Re}(\gamma(\omega))$). This enables the notional direct gap to be determined, $\Delta_{\text{dir}} \simeq 750\omega_L$ here — well separated from the low-energy coherence scale ω_L in strong coupling — and indeed seen to occur for $\epsilon \simeq -\epsilon_c = -0.3$.

The essential points from figure 11 are clear. As expected and well known (see e.g. [11, 12]), significant optical absorption occurs in the vicinity of the direct gap; strongly broadened to low-energies due to electron interactions as above, and all but ‘dead’ on non-universal energy scales (e.g. the hybridization $\Delta_0 = \pi V^2 \rho_0(-\epsilon_c) \sim 7 \times 10^3 \omega_L$ for the chosen bare parameters). Regarding the thermal evolution of the optical conductivity note also that temperatures on the order of a few multiples of the coherence scale ω_L — which control the thermal evolution of the low-energy optics — have essentially no effect on frequencies of the order of the direct gap, reflecting the clean separation between ω_L and Δ_{dir} characteristic of strong coupling. As a corollary the direct gap should be thermally eroded only for $T \sim \mathcal{O}(\Delta_{\text{dir}})$; as indeed seen in figure 12 where (for the same parameters as figure 11) the thermal evolution of $F_{HCL}(\omega; T)$ is shown for temperatures up to $\tilde{T} = 500 \simeq \frac{2}{3}\Delta_{\text{dir}}$. Significant thermal erosion sets in by about $T/\Delta_{\text{dir}} \sim 0.2$ or so, and is well developed by the highest temperature shown. The clear scale separation between ω_L and Δ_{dir} will not however be captured properly if

one is restricted to relatively low interactions and high temperatures as e.g. in quantum Monte Carlo [16,18], or from theories in which the quasiparticle weight Z is algebraically rather than exponentially small in the interaction strength, such as iterated perturbation theory [22,23].

6. Conclusion

We have considered here the periodic Anderson lattice, the canonical model for understanding heavy fermion metals, Kondo insulators, intermediate valence and related materials. Optical conductivities, d.c. transport and single-particle dynamics of the paramagnetic phase have been investigated, using the local moment approach within a DMFT framework. For obvious physical reasons our main focus has been the strongly correlated Kondo lattice regime, where we find the problem to be characterised by a single, exponentially small coherence scale ω_L ; in terms of which the frequency and temperature dependence of physical properties scale — being universally dependent on $\tilde{\omega} = \omega/\omega_L$ and/or $\tilde{T} = T/\omega_L$ regardless of the interaction or hybridization strengths. All relevant energy/temperature scales are handled by the theory, from the low-energy coherent Fermi liquid domain out to large (and in the strict scaling limit arbitrarily large) multiples of ω_L where incoherent many-body scattering dominates the physics; followed by the crossover out of the scaling regime to non-universal, high energy/temperature scales dictated by ‘bare’ model/material parameters. And while our emphasis has been on strong correlations we add that all interaction strengths from weak to strong coupling are encompassed by the LMA [34], such that intermediate valence behaviour in particular can also be addressed.

The first question posed in the Introduction nonetheless remains: to what extent does the model, and our theory for it, capture experiment? We turn to that in the following paper where direct comparison of theory and experiment is made for three heavy fermion materials and a classic intermediate valence compound.

Acknowledgments

We are grateful to the EPSRC for supporting this research.

References

- [1] Grewe N and Steglich F 1991 *Handbook on the Physics and Chemistry of Rare Earths* vol 14 ed K A Gschneider Jr. and L L Eyring (Amsterdam: Elsevier) p 343
- [2] Hewson A C 1993 *The Kondo Problem to Heavy fermions* (Cambridge: Cambridge University Press)
- [3] Aeppli G and Fisk Z 1992 *Comm. Condens. Matter Phys.* **16** 155
- [4] Fisk Z *et al* 1996 *Physica B* **223-224** 409
- [5] Takabatake T *et al* 1998 *J. Magn. Magn. Mater.* **177-181** 277
- [6] Degiorgi L 1999 *Rev. Mod. Phys.* **71** 687
- [7] Riseborough P S 2000 *Adv. Phys.* **49** 257

- [8] Stewart G R 2001 *Rev. Mod. Phys.* **73** 797
- [9] Karnaukhov I N 1997 *Phys. Rev. B* **56** R4313
- [10] Vollhardt D 1993 *Correlated Electron Systems* vol 9 ed V J Emery (Singapore: World Scientific)
- [11] Pruschke T, Jarrell M and Freericks J K 1995 *Adv. Phys.* **44** 187
- [12] Georges A, Kotliar G, Krauth W and Rozenberg M 1996 *Rev. Mod. Phys.* **68** 13
- [13] Gebhard F 1997 *The Mott Metal-Insulator Transition* (Springer Tracts in Modern Physics) vol 137 (Berlin: Springer)
- [14] Shimizu Y and Sakai O 1995 *Computational Physics as a New Frontier in Condensed Matter Research* ed H Takayama *et al* (Tokyo: The Physical Society of Japan) p 42
- [15] Pruschke T, Bulla R and Jarrell M 2000 *Phys. Rev. B* **61** 12799
- [16] Jarrell M 1995 *Phys. Rev. B* **51** 7429
- [17] Tahvildar-Zadeh A N, Jarrell M and Freericks J K 1998 *Phys. Rev. Lett.* **80** 5168
- [18] Tahvildar-Zadeh A N, Jarrell M, Pruschke T and Freericks J K 1999 *Phys. Rev. B* **60** 10782
- [19] Rozenberg M J 1995 *Phys. Rev. B* **52** 7369
- [20] Schweitzer H and Czycholl G 1989 *Solid State Commun.* **69** 179
- [21] Schweitzer H and Czycholl G 1991 *Phys. Rev. Lett.* **67** 3724
- [22] Rozenberg M J, Kotliar G and Kajueter H 1996 *Phys. Rev. B* **54** 8452
- [23] Vidhyadhiraja N S, Tahvildar-Zadeh A N, Jarrell M and Krishnamurthy H R 2000 *Europhys. Lett.* **49** 459
- [24] Grewe N, Pruschke T and Keiter H 1988 *Z. Phys. B: Condens. Matter.* **71** 75
- [25] Pruschke T and Grewe N 1989 *Z. Phys. B: Condens. Matter.* **74** 439
- [26] Cox D L and Grewe N 1988 *Z. Phys. B: Condens. Matter.* **71** 321
- [27] Newns D M and Read N 1987 *Adv. Phys.* **36** 799
- [28] Sun S J, Yang M F and Hong T M 1993 *Phys. Rev. B* **48** 16127
- [29] Burdin S, Georges A and Grepel D R 2000 *Phys. Rev. Lett.* **85** 1048.
- [30] Rice T M and Ueda K 1986 *Phys. Rev. B* **34** 6420
- [31] Fazekas P and Brandow B H 1987 *Physica Scripta* **36(5)** 809
Fazekas P 1987 *J. Magn. Magn. Mater.* **63 & 64** 545
- [32] Smith V E, Logan D E and Krishnamurthy H R 2003 *Eur. Phys. J. B* **32** 49
- [33] Vidhyadhiraja N S, Smith V E, Logan D E and Krishnamurthy H R 2003 *J. Phys.: Condens. Matter* **15** 4045-4087
- [34] Vidhyadhiraja N S and Logan D E 2004 *Eur. Phys. J. B* **39** 313-334
- [35] Logan D E, Eastwood M P and Tusch M A 1998 *J. Phys.: Condens. Matter* **10** 2673
- [36] Glossop M T and Logan D E 2002 *J. Phys.: Condens. Matter* **14** 6737
- [37] Dickens N L and Logan D E 2001 *J. Phys.: Condens. Matter* **13** 4505
- [38] Logan D E and Dickens N L 2002 *J. Phys.: Condens. Matter* **14** 3605
- [39] Logan D E and Glossop M T 2000 *J. Phys.: Condens. Matter* **12** 985
Glossop M T and Logan D E 2003 *J. Phys.: Condens. Matter* **15** 7519
- [40] Bulla R *et al* 2000 *J. Phys.: Condens. Matter* **12** 4899
- [41] Logan D E and Dickens N L 2001 *Europhys. Lett.* **54** 227
Logan D E and Dickens N L 2001 *J. Phys.: Condens. Matter* **13** 9713
- [42] Anderson P W 1961 *Phys. Rev.* **124** 41
- [43] Wachter P 1994 *Handbook on the Physics and Chemistry of Rare Earths* vol 19 ed K A Gschneider and L L Eyring (Amsterdam: Elsevier) p 177
- [44] Nozières P 1985 *Ann. Phys. Fr.* **10** 19
Nozières P 1998 *Eur. Phys. J. B* **6** 447
- [45] Feenberg E 1948 *Phys. Rev.* **74** 206
- [46] Economou E N 1983 *Green's Functions in Quantum Mechanics* (Berlin: Springer)
- [47] Khurana A 1990 *Phys. Rev. Lett.* **64** 1990
- [48] Coleman P 1987 *Phys. Rev. Lett.* **59** 1026